pH of CO_2 saturated water and CO_2 saturated brines

pH of CO_2 saturated water and CO_2 saturated brines: Experimental measurements and modelling

Reza K.Haghi[a], Antonin Chapoy[a,b,*], Luís M. C. Pereira[a], Jinhai Yang[a] , Bahman Tohidi[a]

[a] *Hydrates, Flow Assurance & Phase Equilibria Research Group, Institute of Petroleum Engineering, Heriot-Watt University, Edinburgh EH14 4AS, Scotland, UK*

[b] *Mines Paristech, CTP – Centre Thermodynamique des procédés, 35 rue St Honoré 77305 Fontainebleau, France*

Abstract

In this work, both spectroscopic and electrometric methods were employed to measure the pH of water saturated with carbon dioxide at pressures up to 6 MPa, temperature ranges from 293.15 to 353.15 K and salinities up to 3 mol·kg^{-1}.

Furthermore, a model was developed to predict the changes in the pH due to the solubility of CO_2 in the aqueous phase at high pressure and high temperature conditions as well as the effect of NaCl. The pH model was developed by coupling the Cubic-Plus-Association Equation of State (CPA EoS) and the Pitzer equations. The former was used to determine the solubility of acid gases in aqueous solutions while the latter was employed to calculate activity coefficients for each ion species. The predictive capability of the pH model was evaluated against the data gathered from the literature and data measured in this work. The model allowed a prediction of the pH with an overall average absolute deviation (AAD) to measured data of 0.03 and 0.06 pH units in the CO_2-H_2O system using electrometric and spectroscopic techniques, respectively, and between 0.04 and 0.10 pH units in the CO_2-H_2O-NaCl systems by employing the spectroscopic technique.

KEYWORDS: pH; Carbon dioxide; Water; Sodium chloride

* Corresponding author: E-mail: a.chapoy@hw.ac.uk

1. Introduction

Atmospheric concentration of CO_2 has increased steadily from around the time of the industrial era. This increase in concentration of CO_2 can cause serious global warming and climate change issues. Hence, expanding the methods for removing CO_2 from atmosphere has become an important topic. In the last decades, this issue has prompted researchers to identify methods to combat global warming. Carbon Capture and Storage (CCS) is a set of technologies aimed at alleviating the increase of CO_2 in the atmosphere. Currently, injecting CO_2 at high pressures in deep geologic formations, such as oil and gas reservoirs and deep saline aquifers, is the main alternative strategy for permanent or mid-term disposal of CO_2 instead of releasing it into the atmosphere.

The concepts of pH and pH scales were introduced at the beginning of the last century, and they have since been the most important parameters used to describe the acidity or basicity of aqueous solutions. Since determining of pH is essential for different applications such as marine, pharmaceutical and petroleum industries (Babić et al., 2007; Gray et al., 2011; Millero et al., 2009).In the CCS contexts, the CO_2 injection will cause many chemical reactions as well as hydrodynamic and mechanical changes (Gaus, 2010). As the formation water in deep geological formations (i.e., deep saline aquifers) contains salts, measuring the pH in saline water is a prerequisite to characterise the properties of solutions. For instance, the pH level starts to drop in brine solutions due to CO_2 dissolution and formation of carbonic acid in the reservoir as a result of the CO_2 injection. This variation in pH value in water might cause corrosion of metallic materials in oil and gas wells and can also lead to mineral dissolution/precipitation and scaling in pipelines transporting oil field waters (Crabtree et al., 1999; Gray et al., 1989). Moreover, low values of pH can have a substantial impact on the capture, storage and transportation of CO_2 due to the changes in the porosity and permeability of the reservoir rock (Carroll et al., 2011). Hence, it is necessary to understand the interactions between CO_2 and brine at downhole wellbore conditions (high pressure and temperature) to prevent the formation of scale, corrosion and precipitation of minerals in pipelines as well as for safety concerns in the downhole/wellbore region.

The electrometric technique is typically the most common method for pH measurement. Different types of high pressure and high temperature glass electrodes are commercially available to determine pH of aqueous samples under relevant conditions of temperature and pressure. These glass and reference electrodes require careful handling, particularly during depressurization. Significant amounts of CO_2 can dissolve into the electrode filling solution

when CO_2 is injected into the high pressure cell. Therefore it is necessary to depressurize the system slowly to avoid electrode damage because of a sudden drop in pressure. Furthermore, liquid junction potential is still one of the main drawbacks of this type of measurement, particularly when the sample comprises a large amount of salt. When two different electrolyte solutions come into contact with each other, liquid junction potential may occur between these solutions resulting in an inaccurate pH measurement (Kakiuchi, 2011); several methods have been suggested for decreasing the liquid junction potential (Shibata et al., 2010; Yamada et al., 2015). Another disadvantage of this approach is that it is necessary to calibrate the glass electrode frequently before each measurement using buffer solutions.

Spectroscopic techniques are the alternative technique for precise measurement of pH in CO_2-brine-mineral systems. However, this technique requires the introduction of a specific quantity of dye indicator into the aqueous phase for both calibration and testing samples. Furthermore, each dye indicator covers a limited pH range; nonetheless mixtures of dye indicators at specific concentrations can be prepared, in order to cover the required pH range. Unlike the electrometric method, in the spectroscopic method, it is not necessary to calibrate the system for pH measurement each time before the measurement using buffer solutions.

A number of researchers have shown that optical and electrometric techniques can be used to measure the pH of CO_2 in water and brine at high pressures and temperatures with high accuracy. Meyssami et al. (1992) measured the pH of CO_2 in various fluid systems using a pH probe that was placed inside a high-pressure vessel. They performed all the measurements at pressures up to 35 MPa and temperatures from 305 K to 315 K. An experimental investigation was carried out by Rosenqvist et al. (2012) to measure the pH of water and mineral suspension solution containing dissolved CO_2 using a pH probe at pressures up to 1 MPa and temperature of 294 K. The measured pH values in deionised water were in good agreement with those reported in the literature. Schaef et al. (2003) reported the use of an electrometric technique to determine the pH of both CO_2 saturated H_2O and NaCl systems at pressures up to 11 MPa and temperatures up to 343 K. In this study, the molality of the NaCl solution varied from 1 to 4.49 $mol \cdot kg^{-1}$ (m). Recently, the pH of the CO_2-H_2O system was measured at temperatures between 308 K and 423 K and pressures up to 15 MPa by Peng et al. (2013). They used a commercially-available pH and Ag/AgCl electrodes mounted inside a high-pressure/high-temperature equilibrium cell. All the measured values were compared with a chemical equilibrium model, and a good agreement was obtained between the experimental and simulated data.

The applicability of ultraviolet-visible spectrometer to determine the pH of different fluid systems was investigated by a few research groups. Toews et al. (1995) developed a spectrometer analyser to determine the pH in the CO_2-H_2O system by observing the change in the spectra of the dye indicator (Bromophenol Blue, BPB hereafter) at two specific wavelengths (430 and 590 nm). Measurements were performed at pressures up to 20 MPa and 343K. In this study, the effect of a change in pressure on dissociation constant was neglected for pH calculation. Parton et al. (2002) also employed UV-Vis spectroscopic technique to determine pH in the CO_2-H_2O system at different pressure and temperature conditions. Several spectroscopic studies have been carried out to measure the pH in seawater at atmospheric pressure. Millero et al. (2009) reported the use of spectrometric techniques by dissolving m-cresol purple indicator in NaCl solutions to measure dissociation constants as a function of NaCl molality (0 to 5.5 m) and temperatures (278 to 318 K) at atmospheric pressure. They have provided an equation to calculate the pH based on the dissociation constant of m-cresol purple in brine. These results confirmed the applicability of the spectroscopic method to measure the pH at high level salinities at high temperatures. Recently, Shao et al. (2013) employed the UV-Visible spectrometer to measure the pH in the CO_2-H_2O and CO_2-H_2O-NaCl systems in the presence of two chromophores, BPB and bromocresol green (BCG) which can cover the pH range between 2.5 and 5.2. The experimental values were in good agreement with those obtained through geochemical models. The maximum difference of the experimental data from four different models was found to be 0.16 pH units (Shao et al., 2012). They led to the conclusion that by selecting a suitable calibration procedure and appropriate dye indicators the spectroscopic technique can provide an accurate and precise pH value for the rock−CO_2−brine systems. Truche et al. (2016) reported the pH values in the CO_2-H_2O and CO_2-H_2O-NaCl in a 1.4 molal (m) NaCl solution systems by combining the Raman spectroscopy and the electrometric techniques at temperatures up to 553.15K and pressures up to 15 MPa. Furthermore, they introduced a new thermodynamic model by coupling a Pitzer specific-ion-interaction aqueous model with the Phreeqc geochemical code (Parkhurst and Appelo, 1999). Good agreement was obtained between the model and the experimental data for the CO_2-H_2O-1.4m NaCl system at elevated pressures and temperatures.

To our knowledge, there are very limited experimental studies of pH in the CO_2-brine systems, required to validate and improve the accuracy of model predictions. Hence, investigations of pH in CO_2-brine solutions, particularly at high pressures and high salinities, can greatly improve our knowledge about the change of pH after injecting CO_2 into deep ocean or saline

aquifers. The aim of the present research is to: (1) measure the pH of the CO_2-H_2O systems at pressures around 5.1 MPa and at temperatures up to 353.15 K using a commercially-available pH glass electrode; (2) spectroscopic measurement of pH in different fluid systems (i.e., CO_2-H_2O and CO_2-H_2O-NaCl) using BPB indicator which typically cover the appropriate pH range at pressures up to 6 MPa and temperatures up to 323.15 K ; (3) finally, compare all the experimental results from both methods and the literature data with the developed thermodynamic model.

2. Theory of Spectroscopic Method for pH Measurements

Changes in the colour of the dye indicator will result in a change in the absorbance spectra of protonated (HI^-) and deprotonated (I^{2-}) of the dye indicator. These indicators could exist in both the acid and base form, and the absorbance of light varies while the pH of the solution changes within a certain range of the pH value. The equilibrium between the protonated (acid) and deprotonated (base) of the dye indicator is utilised to measure the pH of the solution.

$$A\,(aq) \leftrightarrows B\,(aq) + H^+ \tag{1}$$

$$pH = pK'_a + \log\frac{\gamma_B}{\gamma_A} + log\frac{[B]}{[A]} = pK_a + log\frac{[B]}{[A]} \tag{2}$$

Where A is the acid form of the dye indicator, B represents the indicator's base form and pK_a is equal to $-\log(K'_a\frac{\gamma_A}{\gamma_B})$ (K'_a is the dissociation constant of the BPB, $\gamma_B$and γ_A are the activity coefficients of base and acid form of the BPB) (Mathews et al., 2009; Raghuraman et al., 2006). BPB solutions exhibit clear changes in their absorbance while the pH value is changing from approximately 2.5 to 4.5. It was observed that BPB absorbs the visible part of spectrum maximally at a wavelength of 440 nm (λ_1) when it is in the acid form and the base form of BPB absorbs the visible light maximally at a wavelength of 590 nm (λ_2). Change in the pH of the solution that containing BPB results in a change in the relative heights of the absorption peaks at these two wavelengths that one corresponds to the concentration of the acid form and other corresponds to the concentration of the base form of the dye in the solution. Eq. (2) must be modified based on the spectral measurements. The absorbance spectrum of BPB in the acid form overlaps with the absorbance spectrum of BPB in the base form at a wavelength of 440 nm (A (λ_1)). Thus, it is required to consider the small amount of the base form in the acid wavelength (See Fig. S1). The same modification requires being considered for the base wavelength (A (λ_2)). This can be performed by applying the Beer-lambert Law.

$$c_{Total} = c_A + c_B \tag{3}$$

c_A and c_B are the concentration of the acid form and the base form of the dye indicator into the sample in mol·kg^{-1}.

$$A(\lambda_1) = \varepsilon_A^{\lambda_1} \cdot c_A \cdot l + \varepsilon_B^{\lambda_1} \cdot c_B \cdot l \quad (4)$$

$$A(\lambda_2) = \varepsilon_A^{\lambda_2} \cdot c_A \cdot l + \varepsilon_B^{\lambda_2} \cdot c_B \cdot l \quad (5)$$

$$R_{\lambda_1}^{\lambda_2} = \frac{A(\lambda_2)}{A(\lambda_1)} \quad (6)$$

$$\frac{c_B}{c_A} = \frac{R_{\lambda_1}^{\lambda_2}\left(1-\frac{\varepsilon_A^{\lambda_2}}{\varepsilon_A^{\lambda_1}\times R_{\lambda_1}^{\lambda_2}}\right)}{\frac{\varepsilon_B^{\lambda_2}}{\varepsilon_A^{\lambda_1}}\left(1-\frac{\varepsilon_B^{\lambda_1}\times R_{\lambda_1}^{\lambda_2}}{\varepsilon_B^{\lambda_2}}\right)} \quad (7)$$

$\varepsilon_A^{\lambda_i}$ and $\varepsilon_B^{\lambda_i}$ are the molar absorptivity of the acid and base form at wavelengths of 440 nm and 590 nm respectively, $R_{\lambda_1}^{\lambda_2}$ is the absorbance ratio and l is the path length, the distance that light travels through the sample. By modifying Eq. (2), one can calculate the pH of a buffer solution:

$$pH = pK_a(t,p,\mu) + log\frac{R_{\lambda_1}^{\lambda_2} - \frac{e_A^{\lambda_2}}{e_A^{\lambda_1}}}{\frac{e_B^{\lambda_2}}{e_A^{\lambda_1}} - R_{\lambda_1}^{\lambda_2}\cdot\frac{e_B^{\lambda_1}}{e_A^{\lambda_1}}} \quad (8)$$

$$e_1 = \frac{e_A^{\lambda_2}}{e_A^{\lambda_1}} \qquad e_2 = \frac{e_B^{\lambda_2}}{e_A^{\lambda_1}} \qquad e_3 = \frac{e_B^{\lambda_1}}{e_A^{\lambda_1}} \quad (9)$$

Where e_1, e_2 and e_3 are the ratio of the molar absorptivity of the protonated (acid) and deprotonated (base) of BPB at two wavelengths (λ_1 & λ_2). A detailed description of the employed theory can be found in the literature (Clayton and Byrne, 1993; Raghuraman et al., 2006; Robert-Baldo et al., 1985; Zhang and Byrne, 1996). pK_a is defined as a function of temperature, pressure and ionic strength. The sensitivity of temperature and ionic strength on the pK_a can be examined experimentally. Furthermore, the effect of pressure on the dissociation constant (K_a (t,p,μ)) can be derived using following equation.

$$\frac{RT}{(P-1)}\ln\frac{K_a(t,p,\mu)}{K_a(t,1,\mu)} = -\Delta V + \Delta k\,\frac{P-1}{2} \quad (10)$$

Where $K_a(t,1,\mu)$ is the dissociation constant of BPB at atmospheric pressure (0.1 MPa). R is the gas constant (8.3144 J mol^{-1} K^{-1}) and, P and T are the pressure and temperature of the fluid system inside the measurement cell. The value of volume changes (ΔV) and compressibility changes (Δk) for BPB were reported by Usha and Atkinson (1992). Using these values, one can solve Eq. (10) to get the dissociation constant of the BPB at various pressures. The

procedure that followed to determine the pK_a and e-values experimentally are discussed in details in the section 5.1.

2.1 Material

The details of the materials used in this study are tabulated in Table 1. All the solutions were prepared using deionised water. For solutions with zero salinity, the glass electrode was calibrated using certified buffer solutions with pH of 4 (citric acid / sodium hydroxide / sodium chloride solution) and 7 (potassium dihydrogen phosphate / disodium hydrogen phosphate). For 1, 2 and 3 $mol \cdot kg^{-1}$ NaCl solutions, Tris buffer (Trizma® base / Trizma® hydrochloride) and HCl solutions with the same NaCl ionic strength were used for calibration of the glass electrode.. Certified buffer solutions with pH of 4 and 7 were provided by Sigma-Aldrich and Hanna instruments. Nitrogen and deionised water were also used for cleaning purposes.

Table 1 Suppliers and specification as stated by the supplier of the materials used in this work.

Chemical name	Source	Purity
CO_2	Air Liquide	>99.99%
NaCl	Sigma Aldrich	>99.95%
Trizma® base	Sigma Aldrich	>99%
Trizma® hydrochloride	Sigma Aldrich	>99%
BPB	Sigma Aldrich	-

2.2 Apparatus

A UV-Vis-NIR spectrometer (C10082MD, Hamamatsu Ltd.) equipped with a UV/VIS/NIR light source (L10290, Hamamatsu) was used for spectra acquisition between 200 to 1100 nm. The light source was mounted to one end of a spectroscopic cell through a fibre optic cable. Each end of the cell is fitted with windows to allow the light to pass through the sample. The cell windows are designed to work at elevated pressures. All the samples were placed in the high pressure titanium cell which can operate at pressures up to 30 MPa. The setup has been designed to have a maximum working temperature of 353 K. The test cell has an effective optical path length of approximately 1.4 cm and an internal diameter of 5.0 cm and internal volume of about 27 cm^3. The cell is housed in a metallic jacket with fluid circulating through it from a cooling/heating bath. The pressure is measured using a Druck pressure transducer with a pressure range up to 60 MPa and previously calibrated against a dead weight pressure balance. This calibration procedure ensures a standard uncertainty of $U(P)$ = 0.05 MPa (Ahmadi et al., 2017). The temperature inside the cell is measured by a high precision PRT probe inserted into the cell. The temperature is regularly calibrated against a Prema 3040

precision thermometer. This calibration procedure ensures standard uncertainties of U (T) = 0.05 K for the temperature readings. A schematic of the apparatus is shown in Fig. 1.

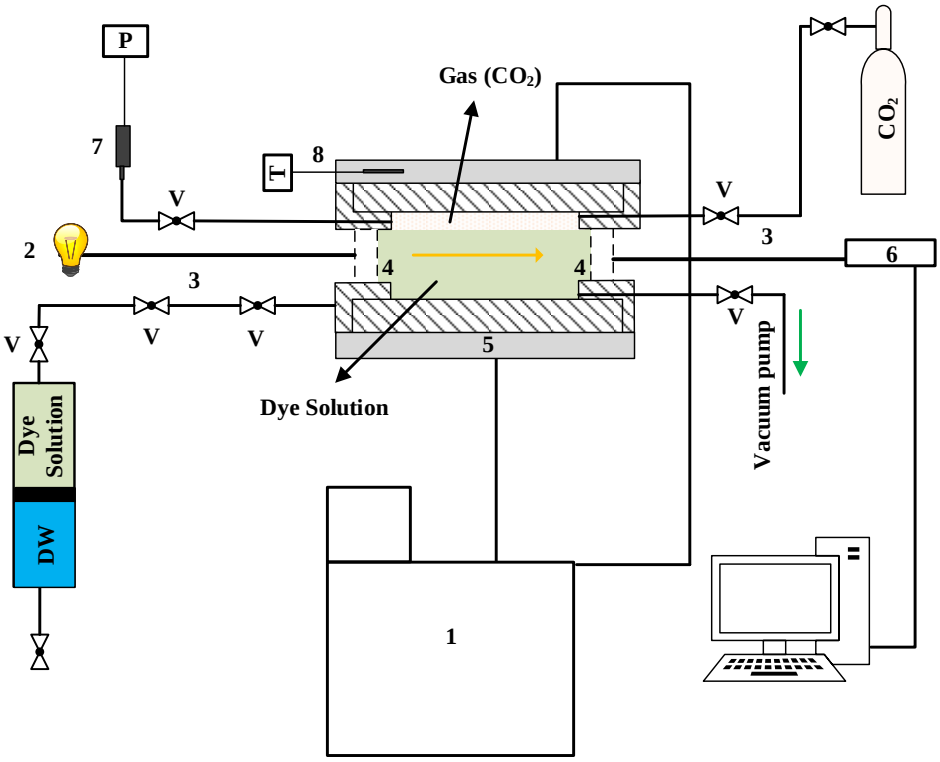

Fig. 1. Schematic diagram of the spectroscopy setup for pH measurements, 1: Cooling / Heating bath, 2: Deuterium and tungsten light sources, 3: Fibre optic, 4: Sapphire windows, 5: High pressure cell, 6: Spectrometer, 7: Pressure transducer, 8: Temperature probe and V: Valve.

2.3 Calibration

Firstly, all the buffer solutions were prepared by combining a specific amount of 0.1 mol·kg^{-1} solution of citric acid and 0.1 mol·kg^{-1} solution of trisodium citrate dihydrate. Various amounts of these stock solutions were combined together in order to reach target pH values. Sodium chloride was then used to set the ionic strength of the buffer solutions to molality of 1, 2 and 3 mol·kg^{-1}. The pH of all the prepared buffer solutions with various ionic strengths at atmospheric pressure and the test temperatures were measured using a pH meter a glass electrode with an Ag/AgCl probe as an internal reference, Hanna, HI-2002 Edge®).

For solutions without NaCl, the glass electrode was calibrated using pH 4 and 7 buffer solutions at 293.15 and 323.15 K. Since the addition of NaCl changes the pH of the prepared buffer solutions, it is required to calibrate the glass electrode using buffer solutions that have the same

ionic strength to determine the actual value of the pH (Marion et al., 2011). For this purpose, 0.05 mol·kg^{-1} Tris buffer solutions (Tris/Tris HCl) and 0.01 mol·kg^{-1} HCl solutions were used to calibrate the glass electrode for NaCl solutions (1, 2 and 3 mol·kg^{-1}) at 293.15 and 323.15 K. The procedure for calibrating the glass electrode for the NaCl solutions is similar to the procedure followed by Peng (2015). The pK_a of 0.05 mol·kg^{-1} Tris/Tris HCl solutions with different NaCl concentrations (0-5 mol·kg^{-1}) at temperatures up to 393.15 K was reported by Foti et al. (1999). Our developed model was used to calculated the pH of 0.01 mol·kg^{-1} HCl solutions at various temperatures and ionic strengths (See Supplementary Information for details). All the prepared buffer solutions were placed into a jacketed beaker connected to a cooling/heating bath. The glass electrode was immersed into the solution at the target temperature. Once the pH value remained constant, the value measured by the pH meter was chosen as the true value for the calibration sample. No significant change was observed in the measured pH value of different buffer solutions for 12 hours (The drift on the e.m.f values was within ± 0.5 mv), showing the high stability of the pH measurement for calibration samples using the glass electrode. All the standard solutions with different ionic strengths were prepared in the pH range between 2.70 and 4.30 to cover the interested pH range within the range of the P–T conditions studied (Fig. 2). After preparing the solutions with different pH and ionic strength values, the high pressure cell was first vacuumed, and 25 ml of each solution was placed into the cell. Then, the temperature of the cell was set at desired temperature, and the spectrum was recorded as a blank spectrum when the desired equilibrium temperature was reached. Afterwards, the BPB dye indicator was dissolved in the same solution at a concentration of 2×10^{-5} mol·kg^{-1}, and the solution was then injected into the cell. A spectrum of the sample was recorded at the same temperature.

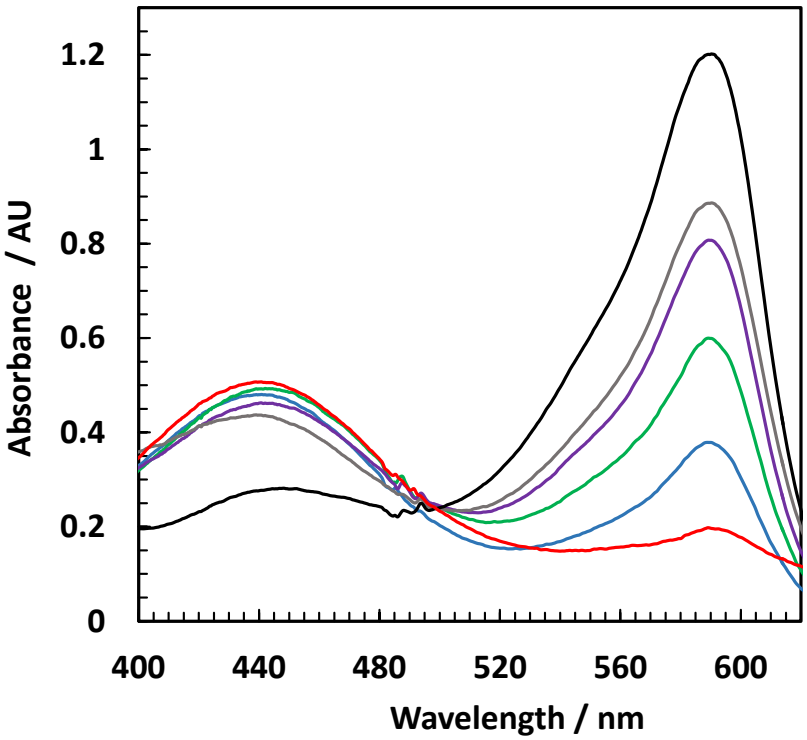

Fig. 2. Spectra of BPB solutions with different pH values at a pressure of 0.1 MPa, the temperature of 298.15 K and zero ionic strength. (2.95 (—), 3.45 (—), 3.65 (—), 3.85 (—),3.98 (—) and 4.25 (—)).

In order to measure the values of e_1, e_2, and e_3 (Eq. 10) experimentally in the absence of the NaCl, a buffer solution with pH of 7 was used as base solution and the pH of the acid solution set to approximately 1.5 by adding about 0.5 mol·kg^{-1} HCl solution to deionised water (Shao et al., 2012). For NaCl solutions, standard solutions with pH of 7 and 1.5 were prepared at each ionic strength (1, 2 and 3 mol·kg^{-1}) to investigate the impact of NaCl concentrations in the BPB solutions on the e-values. The concentration of BPB in all the base and acid solutions (pH =1.5 and 7) was increased and adjusted to about 3×10^{-5} mol·kg^{-1} to obtain the maximum absorbance for the BPB. All the prepared solutions were injected into the cell, and the spectra of the samples were recorded at two different temperatures and atmospheric pressure.

2.4 Experimental procedures

The experimental procedure consists of several steps. In order to record the spectra of different systems, first, the cell was filled with deionised water or brine solutions. When the system reached the desired equilibrium temperature, the spectrum was recorded as a blank. Then, the cell was vacuumed, and it filled with deionised water or brine with a BPB concentration of 2×10^{-5} mol·kg^{-1}. A headspace was left at the top of the cell to allow the gas sample to enter into the cell and dissolve easily into the fluid. Pure CO_2 was then injected to achieve the desired equilibrium pressure. Equilibrium is assumed to have been reached when the total pressure

remains unchanged within 0.007 MPa during a period of 30 minutes. To accelerate the thermodynamic equilibration process, the cell was placed on a pivotal axis, allowing the cell to rock using a compressed air-driven mechanism for each equilibrium condition, the spectrum was recorded three times in order to verify the measurements repeatability and to calculate the standard deviations of the e_1, e_2, e_3 and pK_a.

3. Electrometric Technique for pH Measurements

The electrometric technique is one of the most popular methods for pH measurement in aqueous samples. The principal of electrometric technique is based on the Nernst equation (Bates and Vijh, 1973).

$$E = E^{\circ} - 2.3026 \left(\frac{RT}{F}\right) pH \quad (11)$$

Where R and F are the molar gas constant (8.3144 J mol^{-1} K^{-1}) and the Faraday constant (96.485 kC.mol^{-1}) respectively, T stands for the absolute temperature , E° is the standard electrode potential and E is the measured e.m.f. in the presence of solution (Peng et al., 2013). Different kinds of pH electrodes are available commercially that are suitable for pH measurement over wide ranges of temperature and pressure (Shinwari et al., 2010). One advantage of this method compared to the spectroscopic method is that the calibration procedure is fast and simple but the glass electrode need to be calibrated frequently.

3.1 Apparatus

A high pressure vessel was purchased from Büchi Glas Uster. The cell volume is about 500 cm^3, it is constructed from Hastelloy and wetted parts are corrosive-resistance. The pH measurements were carried out using a glass combination pH probe with an internal standard Ag/AgCl electrode as a reference electrode (Provided by Büchi Glas Uster). The pH probe was mounted through the closure of the vessel as shown in Fig. 3. The glass combination pH probe was designed to operate at pressures up to 6 MPa, and it is capable of being used at temperatures up to 383 K. A pressure transducer was mounted directly on the top of the cell. The system allows real-time readings and storage of pressures during pH measurement. A high pressure magnetic stirrer was used to agitate the test fluids in order to accelerate the process of achieving thermodynamic equilibrium. The cell was surrounded by a cooling jacket connected to a cooling/heating bath for temperature control purposes. A temperature probe was used to monitor the cell temperature. The pH and temperature probes were connected to a controller box that records and displays both pH and temperature.

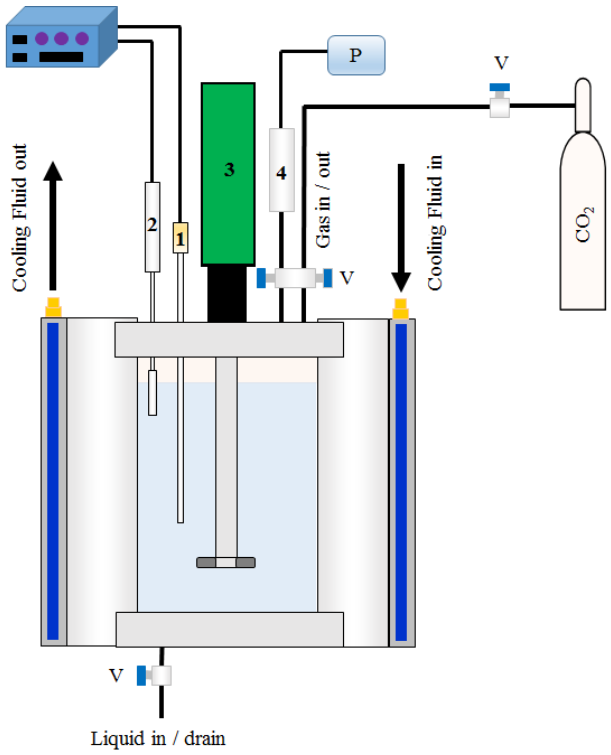

Fig. 3. Schematic diagram of the high pressure setup for pH measurements using the glass electrode, 1: pH probe 2: Temperature probe, 3: Magnetic stirrer, 4: Pressure transducer and V: Valve.

3.2 Calibration

The pressure transducer (ESI technology Ltd) was calibrated against a dead weight pressure balance .The pressure transducer was designed for pressure up to 6 MPa with the uncertainty of U (P) = 0.05 MPa. The cell temperature was measured by a PT100 temperature probe which is located on the upper level of the high pressure cell. The uncertainty of the measured temperature was U(T) = 0.05 K. For solutions with low ionic strengths (less than 0.1 mol·kg^{-1}), certified buffer solutions (pH 7 & pH 4) were used to calibrate the glass electrode on the pH_{NBS} scale (Dickson, 1984; Waters and Millero, 2013). The calibration was performed at atmospheric pressure and three different temperatures (T = 293.15, 323.15 and 353.15 K). The calibration curve for the glass electrode is depicted in Fig. 4. The theoretical slope calculated using the Nernst equation is close to the slope of the calibration curve for the three isotherms. A stable reading on the measured e.m.f. was observed after 12 hours for all the calibration samples (± 0.5 mV).The pH probe was calibrated at every isotherm before starting the pH measurement. To investigate the influence of pressure on the accuracy of calibration, a buffer solution with known pH was placed into the high pressure vessel, and nitrogen was injected to

reach the maximum operating pressure. No significant change was noticed on the pH value of the buffer solution (The drift on the measured e.m.f values was less than 1 mv which is equal to approximately 0.02 pH unit) , showing that pressure does not affect the accuracy of pH measurements. The expanded relative uncertainty for the pH measurement using the electrometric technique in the CO_2-H_2O system was found to be U (pH, k = 2) = 0.07 at 95% confidence level (See appendix for details).

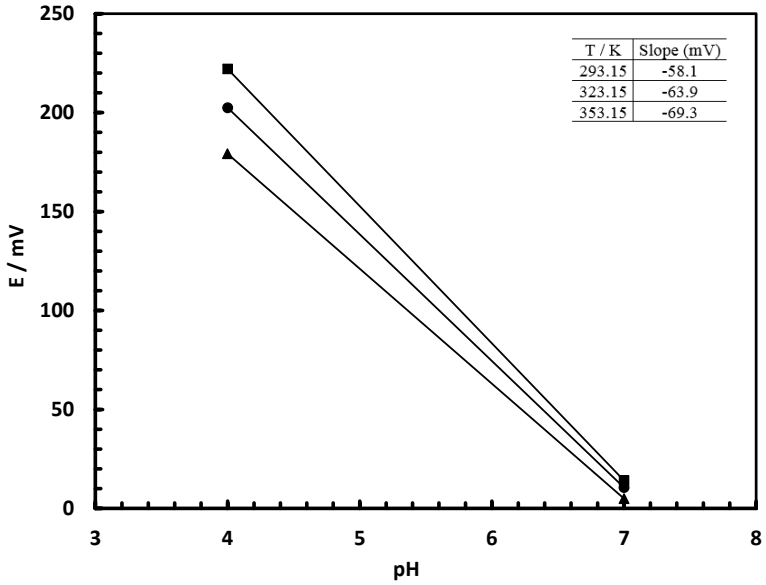

Fig. 4. The e.m.f values measured by the glass electrode for calibration samples at three different temperatures. T = 293.15 K (▲), T = 323.15 K (●) and T = 353.15 K (■).

3.3 Experimental Procedure

Prior to starting the experiments, the entire system was cleaned with deionised water and nitrogen passed through the system to dry the cell, line and valves. Then, the cell was vacuumed, and deionised water was then injected. The cell was initially filled with about 450 cm^3 deionised water. In the next step, CO_2 was introduced to the system. CO_2 was injected slowly at a low rate into in order to avoid electrode damage. The stirrer was set at a low rate (rpm < 50). The pressure, temperature values were monitored and recorded every 5 seconds. Once the pH and pressure remained constant; the value of the pH was recorded. (When pressure, temperature and pH remained constant for a period of 30 minutes).

4. Modelling Approach

In general, most of the recent models have focused on describing the non-ideal behaviour of the systems that arise at HPHT conditions, including both gaseous solubility and description of chemical equilibria of ionic species in solution. In this work the Cubic-Plus-Association Equation of State (CPA EoS) (Kontogeorgis et al., 2006a, b) was selected for determining the solubility of acid gases (CO_2) in pure water and brines at HPHT conditions and the well-known Pitzer's equations (Pitzer, 1973; Pitzer et al., 1984) were coupled for calculating the deviations to the ideality of each ionic species in the liquid phase.

The CPA parameters used for H_2O were taken from Kontogeorgis et al. (1996). Water was modelled using the 4C association scheme (Huang and Radosz, 1990). Critical properties of carbon dioxide were taken from Poling et al. (2001). Binary interaction coefficients (k_{ij}s) within the framework of this EoS were estimated from temperature-dependents functions established in previous works ($k_{CO_2\text{-}H_2O}$(Chapoy et al., 2014; Chapoy et al., 2012)). Carbon dioxide assumed to be able to cross-associate with water (solvation). The effect of salts on the solubility of CO_2 and H_2O are taken into account using the approach proposed by Aasberg-Petersen et al. (1991) and extended to the CPA EoS (Haghighi et al., 2008; Haghighi et al., 2009).

The basic equation used to calculate the pH is defined by:

$$pH = -log_{10}(a_{H^+}) = -log_{10}(m_{H^+}) - log_{10}(\gamma_{H^+}) \quad (12)$$

Where a_{H^+} is the activity (in mol·kg^{-1}), m_{H^+} is the molal concentration (in mol·kg^{-1}), and γ_{H^+} is the activity coefficient (dimensionless) of hydrogen ions.

The equilibrium reactions considered for the systems of interest are as follows:

Pure water and carbon dioxide phase equilibria,

$$H_2O\ (l) \rightleftarrows H^+(aq) + OH^-(aq) \quad (13)$$

$$H_2O\ (l) + CO_2(aq) \rightleftarrows H^+(aq) + HCO_3^-(aq) \quad (14)$$

$$HCO_3^-\ (aq) \rightleftarrows H^+(aq) + CO_3^{2-}(aq) \quad (15)$$

Salts equilibria,

$$NaCl\ (s) \rightleftarrows Na^+(aq) + Cl^-(aq) \quad (16)$$

The thermodynamic equilibrium constants for these reactions are:

$$K_{H_2O} = m_{H^+(aq)}\, m_{OH^-(aq)}\, \frac{\gamma_{H^+(aq)}\, \gamma_{OH^-(aq)}}{a_{H_2O(aq)}} \tag{17}$$

$$K_{CO_2,1} = \frac{m_{H^+(aq)}\, m_{HCO_3{}^-(aq)}}{m_{CO_2(aq)}}\, \frac{\gamma_{H^+(aq)}\, \gamma_{HCO_3{}^-(aq)}}{\gamma_{CO_2(aq)} a_{H_2O(aq)}} \tag{18}$$

$$K_{CO_2,2} = \frac{m_{H^+(aq)}\, m_{CO_3{}^{2-}(aq)}}{m_{HCO_3{}^-(aq)}}\, \frac{\gamma_{H^+(aq)}\, \gamma_{CO_3{}^{2-}(aq)}}{\gamma_{HCO_3{}^-(aq)}} \tag{19}$$

$$K_{NaCl} = m_{Na^+(aq)}\, m_{Cl^-(aq)}\, \gamma_{Na^+(aq)}\, \gamma_{Cl^-(aq)} \tag{20}$$

In order to calculate the pH with Eq. (12), the molality (m_{H^+}) and activity coefficient of the hydrogen (γ_{H^+}) ions need to be determined. Whereas the molality of the ionic species is uniquely given by equilibrium constants of pertinent reactions, the activity coefficients are influenced by all the remaining factors.

In this work, we have followed the Pitzer's formalism (Pitzer, 1973; Pitzer et al., 1984) to determine the activity coefficients present in Eqs. (17 to 20). The Pitzer's model for electrolytes was derived from the Debye-Hückel's method in which the ionic strength and molality of all ionic species in solution are combined to take into account electrostatic interactions between ionic species. The expressions corresponding to this approach will not be addressed here. A detailed description of this methodology can be referred to Pedersen et al. (2014).

The amount of each component in solution is determined by the equilibrium stoichiometric constants and Eqs. (17 to 20). An accurate estimation of these quantities depends on the values considered for the stoichiometric constants. These constants were here determined at each temperature of interest using adjusted mathematical expressions. These adjusted mathematical expressions for water were the recommended expression from the International Association for the Properties of Water and Steam (IAPWS, 2007) and for others from Pedersen et al. (2014). Furthermore, the effect of pressure on these values, excluding water, was neglected. The amount of CO_2 (aq) and the effect of salts on these quantities were calculated with our PVT model based on the CPA EoS.

The molality and activity coefficients for each ionic species are calculated together with the resolution of the equation for electro neutrality, considering no mineral precipitation has occurred, defined as follows:

$$m_{H^+(aq)} - \frac{K_{H_2O}\, a_{H_2O(aq)}}{m_{H^+(aq)}\, \gamma_{H^+(aq)}\, \gamma_{OH^-(aq)}} - \frac{K_{CO_2,1} m_{CO_2(aq)} \gamma_{CO_2(aq)} a_{H_2O(aq)}}{m_{H^+(aq)}\, \gamma_{H^+(aq)}\, \gamma_{HCO_3^-(aq)}} -$$

$$2\frac{K_{CO_2,2}\, m_{HCO_3^-(aq)} \gamma_{HCO_3^-(aq)}}{m_{H^+(aq)}\, \gamma_{H^+(aq)}\, \gamma_{CO_3^{2-}(aq)}} = 0 \qquad (21)$$

The amount of hydrogen ion (m_{H^+}) is calculated by solving Eq. (21) with a Newton-Raphson iteration method and pH determined with Eq. (12).

5. Results and Discussion

5.1 Spectroscopic Technique – (pK_a and molar absorptivity coefficients of the BPB)

As mentioned before, in the spectroscopic method, the measurements were performed at pressures up to 6 MPa and temperatures of 293.15 K and 323.15 K. Some experiments were carried out to investigate the e_1, e_2, and e_3 rates dependence on pressure, temperature and ionic strength. In order to find the influence of pressure on the molar absorptivity ratios, firstly, the spectra of the acid (pH = 1.5) and base solutions (pH = 7) in the presence of BPB were measured. Then, nitrogen was introduced to the system to measure the spectra of the acid and base samples at various pressures (up to 6 MPa). A very small dependence of the molar absorptivity ratios to pressure was noticed and not accounted for the pH calculations. It should be noted that the molar absorptivity coefficients were measured at the calibrated temperatures (293.15 & 323.15 K) as indicated in

Table 2. To examine the influence of a change in salinity on the molar absorptivity ratios values, the spectra of acid and base solutions with different ionic strengths (1, 2 and 3 $mol \cdot kg^{-1}$) at fixed temperature and atmospheric pressure were measured. Results revealed that the changes in the e_1, e_2, and $e_3$values are negligible at different ionic strengths. In terms of the pK_a, various buffer solutions with different ionic strengths were prepared within the range of study. Spectra of all these solutions in the presence of BPB were measured at the atmospheric pressure and two different temperatures. After extracting the λ_1 and λ_2 from the recorded spectra, the pK_a at each ionic strength and isotherm is determined from the intercept of the line with the x-axis using the Eq. (8). It should be noted that all the spectra were baseline corrected between the ranges from 340 to 655 nm before any calculation to overcome baseline shift during measurement. The results for e_1, e_2, and e_3 and pK_a values at different temperatures and ionic strengths at atmospheric pressure are listed in

Table 2.

Table 2 Measured pK_a, e_1 , e_2 and e_3 of BPB at atmospheric pressure and different temperatures and ionic strengths.

T/K	m_{NaCl} / *mol·kg*$^{-1}$	*pK*$_a$	*U***(pK*$_a$*)*	*e*$_1$	*U(e*$_1$*)*	*e*$_2$	*U(e*$_2$*)*	*e*$_3$	*U(e*$_3$*)*
293.15	0	4.115	± 0.016	0.014	± 0.005	2.682	± 0.009	0.022	± 0.005
	1	3.772	± 0.017						
	2	3.791	± 0.017						
	3	3.882	± 0.019						
323.15	0	4.145	± 0.015	0.018	± 0.006	2.712	± 0.009	0.0381	± 0.008
	1	3.751	± 0.015						
	2	3.762	± 0.014						
	3	3.853	± 0.018						

* U denotes the uncertainty. Uncertainties calculations are described in details in the appendix section.

The pK_a values obtained at 293.15 K and 323.15 for different fluid systems were close to those reported by Shao et al. (2012) (See Supplementary Information). Calculated values for pK_a, e_1, e_2 and e_3 were then used to determine the value of pH using the spectra collected for the CO_2-H_2O and CO_2-H_2O-NaCl systems at 298.15 K and 323.15K and pressures up to 6 MPa. The expanded uncertainty for the pH measurement using the spectroscopy technique was found to be 0.09 at 95% confidence level (See the appendix section for details).

5.2 Equilibrium pH of CO_2 in Contact with Water and Brines

In this section, the results obtained experimentally by both the UV-Vis spectroscopic and electrometric techniques with the available data in the open literature within the range of our study are evaluated and compared. Three isotherms for the CO_2-H_2O system were studied in the temperature range of 293.15 to 353.15 K and pressures up to 5.1 MPa using the electrometric technique. For the spectroscopic technique, the pH was measured in the CO_2-H_2O, and CO_2-H_2O-NaCl systems at pressures up to 6 MPa and temperatures up to 323.15 K. The pH results obtained for both the spectroscopic and electrometric techniques in the CO_2-H_2O system are tabulated in

Table 3 and

Table 4 and depicted in Fig. 5 and Fig. 6 respectively. Moreover, all the results were compared with selected data from the literature. As can be seen in Fig. 5, the results that were measured using the pH probe are in quite good agreement with those obtained by Peng et al. (2013), indicating the consistency of this method for pH measurements in CO_2 saturated water. It is

apparent that, for all studied isotherms, the pH value decreases sharply with increasing pressures while the operating pressure is less than 3 MPa. This reduction in pH values is less for pressure higher than 3 MPa. For instance, in this study, pH decreased from 3.88 to 3.41 when the pressure was increased from 0.23 to 2.15 MPa at 323.15 K. However the pH value at the same temperature reduced by 0.15 units from 3.44 MPa to 5.07 MPa. This reduction in the pH value is expected to be less at higher pressures, which can be described by the lower solubility of CO_2 in the liquid phase. A similar trend was observed by Peng et al. (2013) at T = 323.0 K, pH decreased by 0.40 units from 0.38 to 2.43 MPa due to the high solubility of CO_2 in this range of pressure, whereas the pH value fell by 0.22 units while the pressure was increased from 2.43 to 6.23 MPa. Moreover, the results obtained in this study for the spectroscopic technique were compared with the available literature data for the same method within the range of the P–T conditions studied. As illustrated in Fig. 6, the general trend in this method is in good agreement with the data that reported by Shao et al. (2012) and Parton et al. (2002). The measured pH values in this work were close to values obtained by Shao et al. (2012), however, pH results reported at a pressure higher than 2 MPa and T = 308.15 K by Parton et al. (2002) are about 0.2 units lower than values measured in this study at T= 293.15 K. This difference is even higher as they measured the pH at slightly higher temperature (pH values at T = 293.15 K in this study was compared to pH values at T = 308.15 K) which results in an increase in pH value due to the lower solubility of CO_2 at higher temperature. This difference in pH value may be attributed either to the procedure that was followed to calculate the pH or error of measurement. Overall, results obtained in this study by either the spectroscopic and electrometric methods for the CO_2-H_2O system follow a similar trend, fast drop in pH value while pressure is less than 3 MPa and lower changes in pH values at a pressure higher than 3 MPa.

Table 3 Measured and predicted pH values (electrometric technique) in the CO_2-H_2O system.

T/K	*P/MPa*	*pH (Experimental)*	*pH (Model)*
293.15	0.23	3.78	3.77
	0.74	3.53	3.52
	1.45	3.39	3.37
	2.15	3.32	3.29
	3.44	3.23	3.20
	5.07	3.18	3.13
323.15	0.23	3.88	3.86
	0.74	3.61	3.60
	1.45	3.48	3.46
	2.15	3.41	3.38
	3.44	3.32	3.28
	5.07	3.17	3.20

353.15	0.23	4.00	4.02
	0.74	3.70	3.73
	1.45	3.54	3.57
	2.15	3.46	3.49
	3.44	3.36	3.39
	5.07	3.28	3.31

Table 4 Measured and predicted pH values (spectroscopic technique) in the CO_2-H_2O system.

T/K	*P/MPa*	*pH (Experimental)*	*pH (Model)*
T =293.15	0.60	3.58	3.65
	1.51	3.44	3.45
	2.25	3.36	3.27
	2.94	3.28	3.31
	4.41	3.19	3.23
	5.24	3.17	3.20
T = 323.15	1.14	3.59	3.51
	2.16	3.46	3.38
	3.25	3.40	3.29
	4.02	3.31	3.25
	5.51	3.27	3.19

Moreover, all the results were compared with selected data from the literature. As can be seen in Fig. 5, the results that were measured using the pH probe are in quite good agreement with those obtained by Peng et al. (2013), indicating the consistency of this method for pH measurements in CO_2 saturated water. It is apparent that, for all studied isotherms, the pH value decreases sharply with increasing pressures while the operating pressure is less than 3 MPa. This reduction in pH values is less for pressure higher than 3 MPa. For instance, in this study, pH decreased from 3.88 to 3.41 when the pressure was increased from 0.23 to 2.15 MPa at 323.15 K. However the pH value at the same temperature reduced by 0.15 units from 3.44 MPa to 5.07 MPa. This reduction in the pH value is expected to be less at higher pressures, as the changes in the solubility of carbon dioxide is greater relatively at low pressure (at 323.15 K a tenfold increase in the CO_2 solubility is observed from 0.23 to 2.15 MPa, whereas from 3.44 to 5.07 MPa a 40% increase in solubility is observed). A similar trend was observed by Peng et al. (2013) at T = 323.0 K, pH decreased by 0.40 units from 0.38 to 2.43 MPa due to the high solubility of CO_2 in this range of pressure, whereas the pH value fell by 0.22 units while the pressure was increased from 2.43 to 6.23 MPa. Moreover, the results obtained in this study for the spectroscopic technique were compared with the available literature data for the same method within the range of the P–T conditions studied. As illustrated in Fig. 6, the general

trend in this method is in good agreement with the data that reported by Shao et al. (2012) and Parton et al. (2002). The measured pH values in this work were close to values obtained by Shao et al. (2012), however, pH results reported at a pressure higher than 2 MPa and T = 308.15 K by Parton et al. (2002) are about 0.2 units lower than values measured in this study at T= 293.15 K. This difference is even higher as they measured the pH at slightly higher temperature (pH values at T = 293.15 K in this study was compared to pH values at T = 308.15 K) which results in an increase in pH value due to the lower solubility of CO_2 at higher temperature. This difference in pH value may be attributed either to the procedure that was followed to calculate the pH or error of measurement. Overall, results obtained in this study by either the spectroscopic and electrometric methods for the CO_2-H_2O system follow a similar trend, fast drop in pH value while pressure is less than 3 MPa and lower changes in pH values at a pressure higher than 3 MPa.

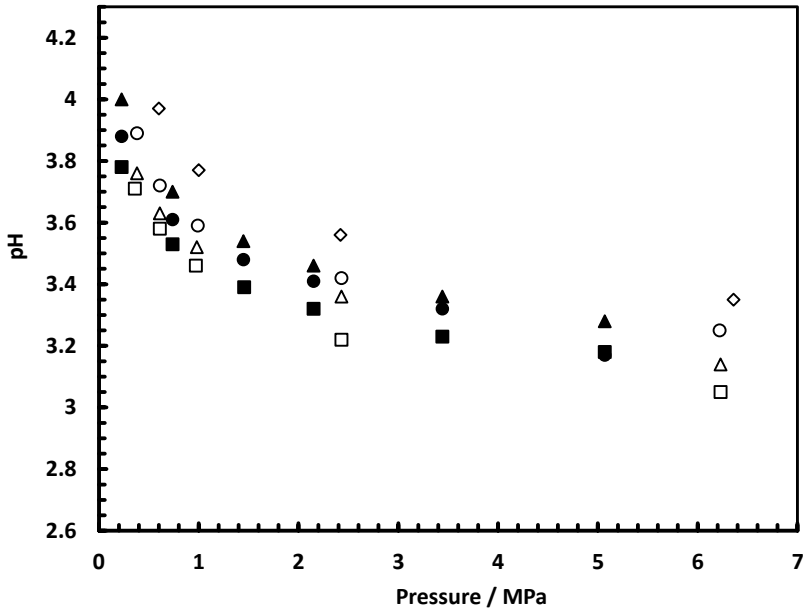

Fig. 5. pH of CO_2 saturated solutions as a function of pressure in the CO_2-H_2O system (Electrometric technique). Filled symbols represent experimental data measured in this work : T = 293.15 K (■), T = 323.15 K (●) and T = 353.15 K (▲). Empty symbols represent the data measured by Peng et al. (2013): T = 308.3 K (□), T = 323.0 K (△), T = 343.0 K (○) and T = 368.1 K (◇).

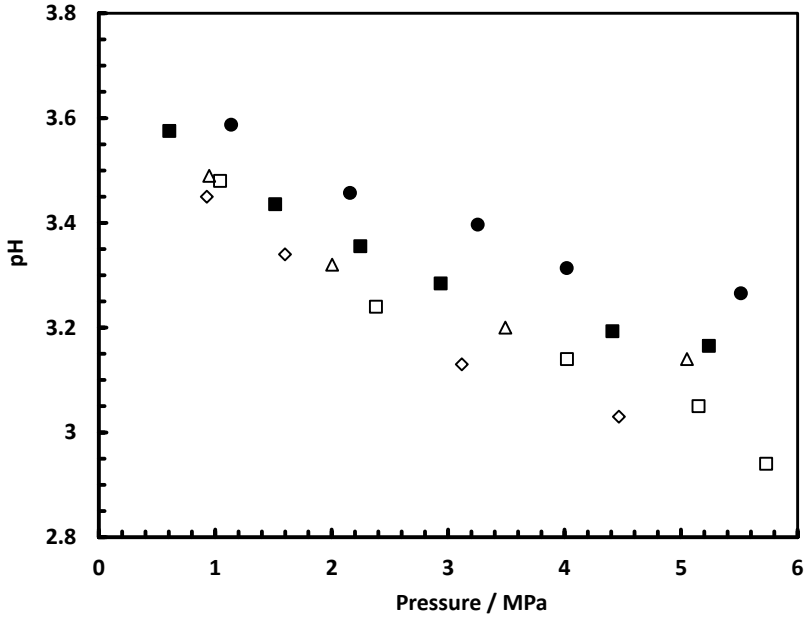

Fig. 6. pH of CO_2 saturated solutions as a function of pressure in the CO_2-H_2O system (Spectroscopic technique). Filled symbols represent experimental data measured in this work: T = 293.15K (■) and T = 323.15 K (●). Empty symbols represent the data measured by Schaef et al. (2003), T = 295.15 (□) ; Parton et al. (2002), T = 308.15 K (◇) and Shao et al. (2012), T = 313.0 K (△).

Some limited data are available for pH in CO_2-brine systems at high pressures. Crolet and Bonis (1983) reported the pH measurements for the CO_2-H_2O-0.5m NaCl system at temperatures from 289.15 to 347.15 K and pressures up to 6 MPa. Shao et al. (2012) and Schaef et al. (2003) measured the pH in CO_2-brine systems at temperatures up to 366.15 K and pressures up to 20 MPa using spectroscopic and electrometric methods respectively. In the current study, pH was measured for aqueous solutions with different ionic strengths (1, 2 and 3 $mol \cdot kg^{-1}$) at temperatures up to 323.15 K and pressures up to 6 MPa. Measured pH values from this study and from those reported in the literature for solutions with different ionic strengths are illustrated in Fig. 7 through Fig. 9. As can be seen from Fig. 7 and Fig. 8, for CO_2-H_2O-1m NaCl and CO_2-H_2O-2m NaCl systems, the measured pH values are lower by about 0.2 to 0.3 unit than those measured by Schaef et al. (2003). Furthermore, it is clear from the aforementioned figures that the pH values reported by Schaef et al. (2003) are increased with an increase in salinity. This opposite trend and also the large difference between the measured pH values from this study and those measured by Schaef et al. (2003) could be due to the occurrence of liquid junction potential between the liquid inside and outside glass electrode which produces some errors in pH measurement. Due to the presence of a high concentration of NaCl in the studied solutions, Na^+ ions can diffuse into the liquid junction and produce an

undesirable potential difference between the filled solution inside the glass electrode and the liquid outside of the glass electrode, causing offset in the pH value.

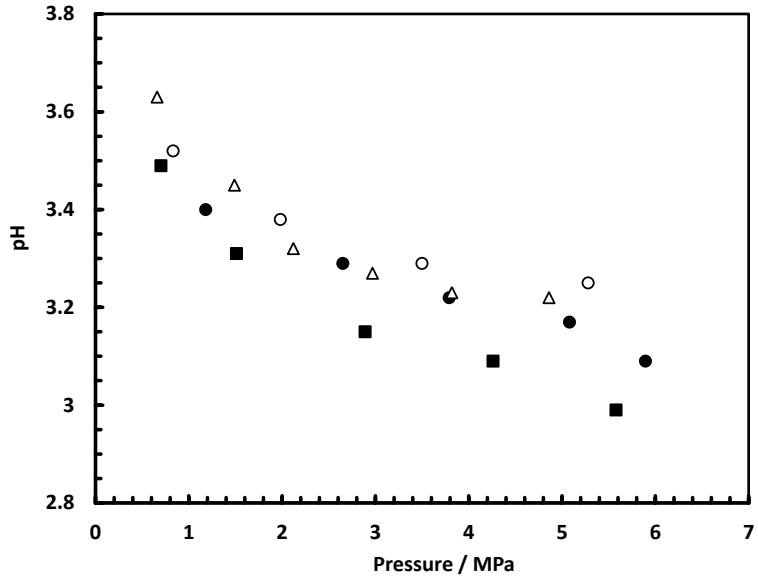

Fig. 7. pH of CO_2 saturated solutions as a function of pressure in the CO_2-H_2O-NaCl system. Filled symbols represent experimental data measured in this work using spectroscopic technique (m = 1 mol·kg^{-1}): T = 293.15K (□) and T = 323.15 K (●).Empty symbols represent the data measured using the electrometric technique by Schaef et al. (2003), (m = 1.03 mol·kg^{-1}): T = 295.15 K (△) T = 313.15K (○).

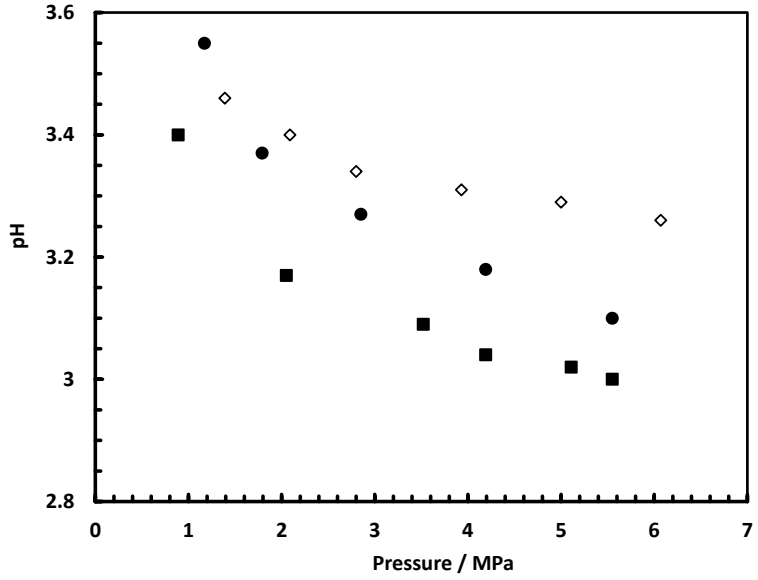

Fig. 8. pH of CO_2 saturated solutions as a function of pressure in the CO_2-H_2O-NaCl system. Filled symbols represent experimental data measured in this work using spectroscopic technique (m = 2 mol·kg^{-1}): T = 293.15K (■) and T = 323.15 K (●). Empty symbols represent the data measured using the electrometric technique by Schaef et al. (2003), (m= 2.11 mol·kg^{-1}): T = 295.15 K (◇).

As depicted in Fig. 9, our measured pH values at T = 323.15 K in the CO_2-H_2O-3m NaCl system is close with data of Shao et al. (2012) at temperature of 313.15 K.

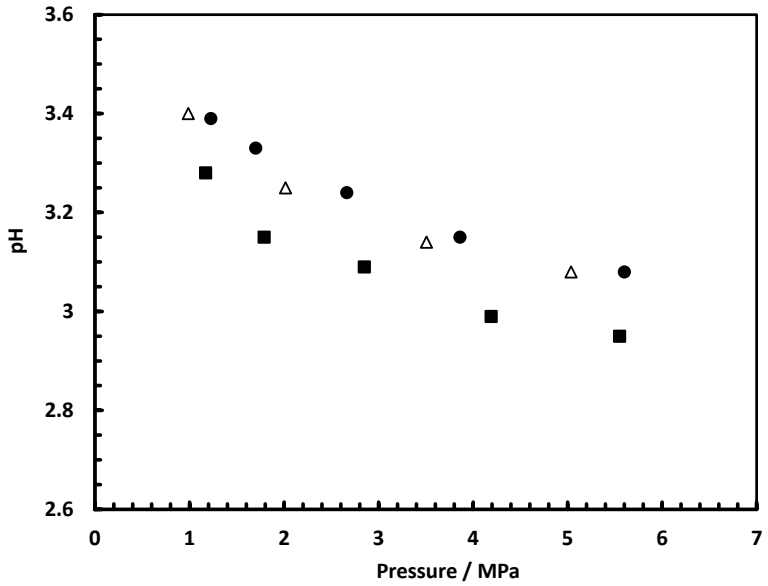

Fig. 9. pH of CO_2 saturated solutions as a function of pressure in the CO_2-H_2O-NaCl system. Filled symbols represent experimental data measured in this work using spectroscopic technique (m = 3 mol·kg^{-1}): T = 293.15K (■) and T = 323.15 K (●).Empty symbols represent the data measured using the spectroscopic technique by Shao et al. (2012) (m = 3 mol·kg^{-1}): T = 313.15 K (△).

It is clear from Fig. 10 that the salinity increase leads to a reduction of pH in acidified brine solutions over the entire pressure range at a constant temperature. This behaviour was more pronounced while the concentration of NaCl changed from 1 to 3 mol·kg^{-1}. For instance, as shown in Fig. 10 and Table 5, the pH drops by about 0.1 units at a pressure of about 5.5 MPa and temperature of 293.15 K. A similar trend was observed by Crolet and Bonis (1983), they measured the pH in CO_2-brine systems (0 to 3.87 mol·kg^{-1}) at 0.1 MPa and T =298.15 K, it was observed that the pH decreases from 3.76 to 3.57 when the ionic strength increases from 1.03 to 3.87 mol·kg^{-1}. It is known that CO_2 solubility decreases with the increase of NaCl concentration in the solution but the activity coefficient (γ_{H^+}) increases significantly with the increase of NaCl concentration in the solution, causing a drop in the pH value (See Supplementary Information for details). However, an opposite trend was noticed by Shao et al. (2012). They showed that the pH value increases in the CO_2-brine systems from 2.94 to 2.98 as the salt concentration increases from 1 to 3 mol·kg^{-1} at a pressure of 10 MPa and T = 313.15 K.

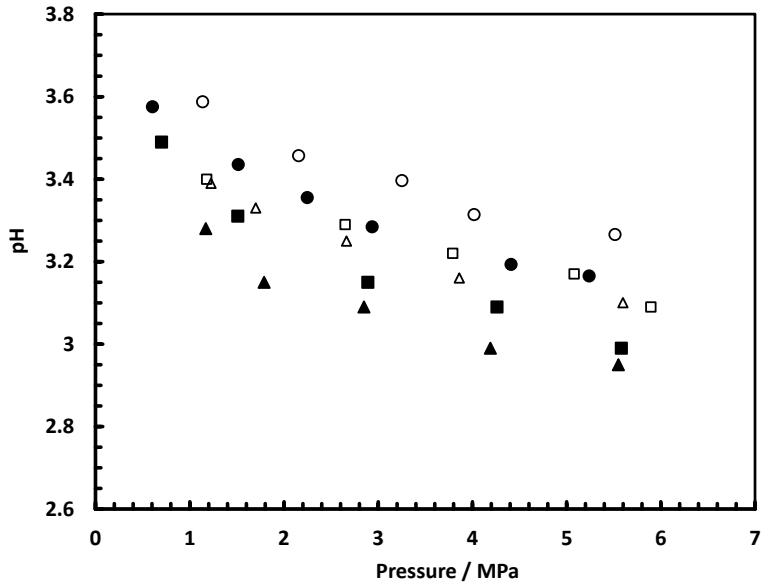

Fig. 10. Effect of variation in ionic strength on the pH value of the CO_2 saturated solutions as a function of pressure (spectroscopic technique). T = 293.15 K; 0m NaCl (●), 1m NaCl (■) and 3m NaCl (▲). T =323.15 K; 0m NaCl (○), 1m NaCl (□) and 3m NaCl (△).

Table 5 Measured and predicted pH value (spectroscopic technique) for different CO_2 saturated brine systems.

T/K	*P/MPa*	m_{NaCl} *(mol·kg^{-1})*	*pH (Experimental)*	*pH (Model)*
T =293.15	0.70	1	3.49	3.42
	1.51	1	3.31	3.25
	2.89	1	3.15	3.12
	4.26	1	3.09	3.05
	5.58	1	3.04	3.00
T = 323.15	1.18	1	3.40	3.42
	2.65	1	3.29	3.25
	3.79	1	3.22	3.18
	5.08	1	3.17	3.13
	5.90	1	3.12	3.10
T = 293.15	0.89	2	3.40	3.28
	2.05	2	3.17	3.10
	3.52	2	3.09	3.00
	4.19	2	3.04	2.97
	5.11	2	3.02	2.93
	5.55	2	3.00	2.90
T = 323.15	0.85	2	3.55	3.43
	1.57	2	3.37	3.30
	2.99	2	3.27	3.17
	4.45	2	3.18	3.10
	5.63	2	3.12	3.06
T = 293.15	1.17	3	3.28	3.14
	1.79	3	3.15	3.05
	2.85	3	3.09	2.96
	4.19	3	2.99	2.89
	5.55	3	2.95	2.84
T = 323.15	1.23	3	3.39	3.30
	1.70	3	3.33	3.23
	2.66	3	3.24	3.14
	3.86	3	3.15	3.07
	5.60	3	3.08	3.00

5.3 Modelling Results

The pH predictions calculated with our model were evaluated against literature data and these new measurements. Summary of the calculated AAD value (Average of all absolute deviations) between the predicted pH values by the model and the available experimental data in the open literature as well as the experimental data obtained in this study are listed in Table 6.

Table 6 Summary of the calculated AAD value between the pH measured and predicted values in various fluid systems.

System	Data Source	T/K	P/MPa	NP[a]	AAD[b]
CO_2-H_2O	Peng et al. (2013)	308.3 to 423.2	0 to 15	37	0.04
	Shao et al. (2012)	298.15 to 366.15	0 to 20	18	0.03
	Truche et al. (2016)	423.15 to 553.15	0 to 15	14	0.06
	Schaef et al. (2003)	295.15 to 343.15	0 to 11	12	0.19
	Meyssami et al. (1992)	305.15 to 315.15	0 to 35	26	0.06
	Toews et al. (1995)	298.15 to 343.15	7 to 20	20	0.24
	Parton et al. (2002)	308.15	0 to 9	6	0.09
	Rosenqvist et al. (2012)	294	0 to 1	3	0.07
	This work, ET[c]	293.15 to 353.15	0 to 6	18	0.03
	This work, ST[d]	293.15 to 323.15	0 to 5.5	11	0.06
CO_2-H_2O-1.02 m NaCl	Schaef et al. (2003)	295.15 to 343.15	0 to 10	25	0.14
CO_2-H_2O-1m NaCl	This work, ST	293.15 to 323.15	0 to 6	10	0.04
CO_2-H_2O-2.11m NaCl	Schaef et al. (2003)	295.15 to 343.15	0 to 11	9	0.32
CO_2-H_2O-2m NaCl	This work, ST	293.15 to 323.15	0 to 6	11	0.09
CO_2-H_2O-3m NaCl	Shao et al. (2012)	298.15 to 366.15	0 to 20	18	0.05
	This work, ST	293.15 to 323.15	0 to 6	10	0.10

[a] Number of points

[b] $AAD = \frac{1}{NP} * \sum_1^{NP} \left| (pH_{Model} - pH_{Exp}) \right|$

[c] Electrometric Technique

[d] Spectroscopic Technique

It can be seen from Table 6 the predicted pH values by the model provide a good representation of the measured data at pressures up to 6 MPa with an average absolute deviations (AAD) of 0.03 pH units for the electrometric method in the temperature ranges from 293.15 to 353.15 K and AAD of 0.06 pH units for the spectroscopic method in temperatures up to 323.15 K.

Moreover, the accuracy of the model was investigated against values reported in the literature for pH in the CO_2-H_2O system at elevated temperatures and pressures. As can be seen from Fig. 11 and Fig. 12, the pH appears to abruptly decrease with pressure increase while this reduction in pH value at pressures higher than 10 MPa is very small. The model is able to predict the pH value in CO_2 saturated water system with an AAD of 0.04, 0.03 and 0.06 pH units to experimental points that were reported by Peng et al. (2013), Truche et al. (2016) and Shao et al. (2012) respectively at pressures up to 20 MPa and temperatures up to 553 K. Furthermore, the measured pH values by Toews et al. (1995) are about 0.2-0.3 units lower than pH values predicted by the model at same P-T conditions (see Fig. 12, AAD = 0.24 pH units). A possible reason behind this large difference between the model and measured pH values is because the impact of pressure and ionic strength were not considered in their calibration procedure. They reported the pH values for pressures between 7 MPa and 20 MPa in the CO_2-H_2O system. As can be seen in Fig. 12, the changes in pH are very small at pressures higher than 7 MPa (about 0.03 units). Similar behaviour was observed in the model, the pH decreased by about 0.06 units while the pressure increases from 7 MPa to 20 MPa at a temperature of 298.15 K. This behaviour is closely linked to the amount of molecular CO_2 in the liquid phase (x_{CO_2}).

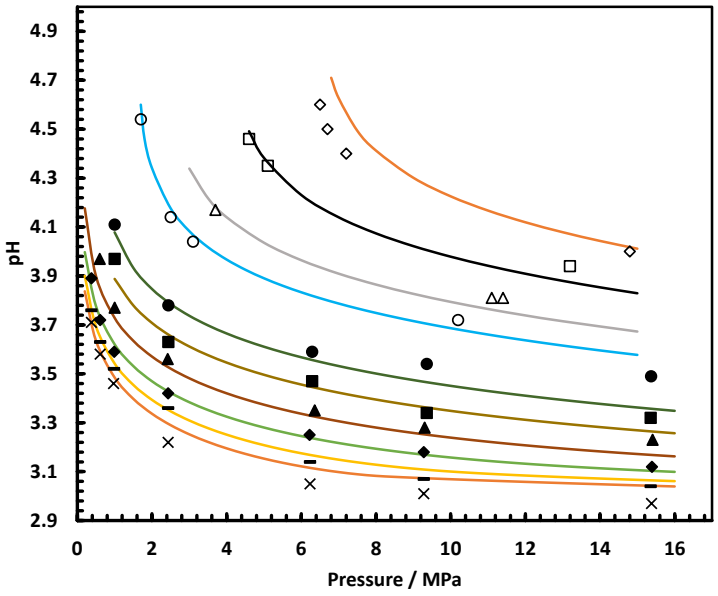

Fig. 11. pH of CO_2 saturated solutions as a function of pressure in the CO_2-H_2O system. Symbols represent experimental data from the literature: Peng et al. (2013) : T = 308.3 K (×), T = 323 K (–), T = 343 (◆) T = 368.1 (▲) T = 398.3 (■) T = 423.2 (●). Empty symbols represent results that obtained by Truche et al. (2016) : T = 473.15 K (○), T = 493.15 K (△), 523.15 K (□) and 553.15 K (◇). Solid lines represent the prediction from the model: T = 308.30 K (–), T = 323 K (–), T = 343 (–) T = 368.1 (–) T = 398.3 (–) T = 423.2 (–) T = 473.15 K (–), T = 493.15 K (–), 523.15 K (–) and 553.15 K (–).

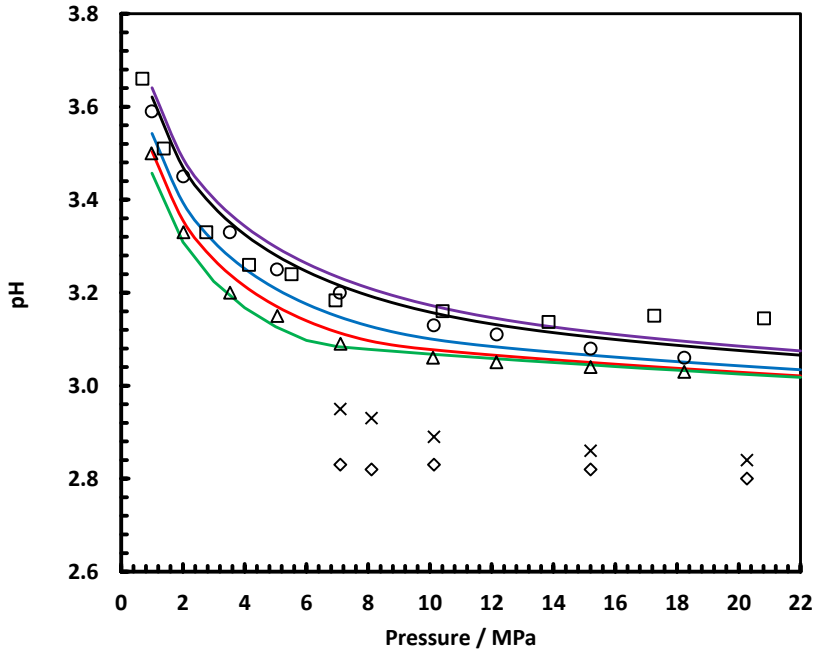

Fig. 12. pH of CO_2 saturated solutions as a function of pressure in the CO_2-H_2O system. Empty symbols represent experimental data from the literature: Meyssami et al. (1992), T = 315.15 K (□); Shao et al. (2012), T = 348.15 K (○); Shao et al. (2012), T = 313.15 K (△);.Toews et al. (1995), T = 343.15 (×) and Toews et al. (1995), T = 298.15 (◇). Solid lines represent the prediction from the model: T = 298.15 (—), T = 313.15 K (—), T = 323.15 K (—), T = 343.15 (—) and T = 348.15 (—).

In Fig. 13, one can see a steep increase in the composition of CO_2 for pressures up to 10 MPa and a moderate rise in this quantity for higher pressures. Such singularity produces small changes in the concentration of the CO_2 in the aqueous phase. As depicted in Fig. 13, the pH values seem to level off for higher pressures. We also plot the pH of the CO_2-H_2O system as a function of $-\log_{10}(x_{CO_2})$ (Fig. 14). A linear relationship was observed between pH and $-\log(x_{CO_2})$ for the CO_2 saturated water system.

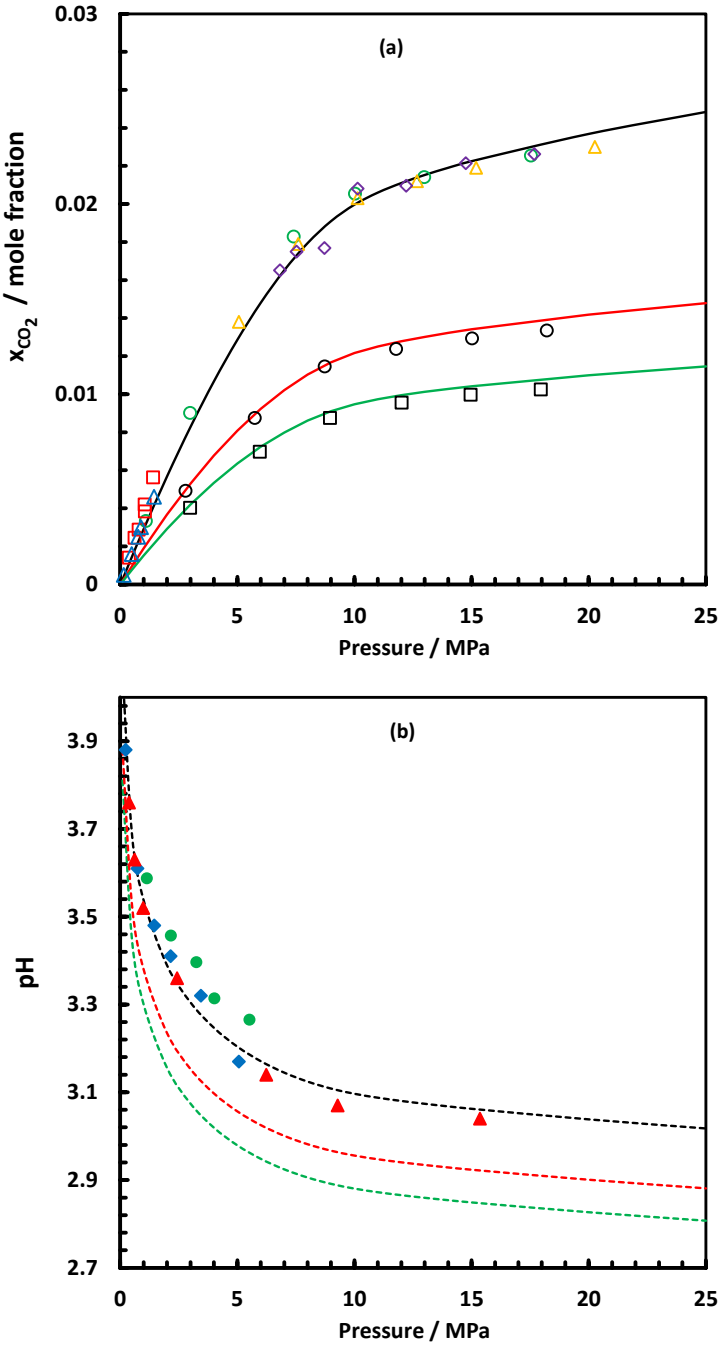

Fig. 13. x_{CO_2}-pressure (a) and pH-pressure (b) diagrams of the CO_2-H_2O and CO_2-H_2O-NaCl systems at temperature of 323.15 K. Empty symbols represent experimental mole fraction data of CO_2 in aqueous phase: 0 m NaCl (□), Zaalishvili (1940); 0 m NaCl (△) Zawisza and Malesinska (1981); 0 m NaCl (○), Hou et al. (2013a); 0 m NaCl (△), Wiebe (1941); 0 m NaCl (◇), Briones et al. (1987); 2.5 and 4 m NaCl (○ and □), Hou et al. (2013b). Filled symbols represent experimental pH data : 0 m NaCl (▲), Peng et al. (2013); 0 m NaCl (●), this work (Spectroscopic technique) and 0 m NaCl (◆),this work (Electrometric technique). Dashed and solid lines represent the pH and x_{CO_2} predictions at various temperatures from the model respectively (0 m NaCl (black), 2.5 m NaCl (red) and 4 m NaCl (green)).

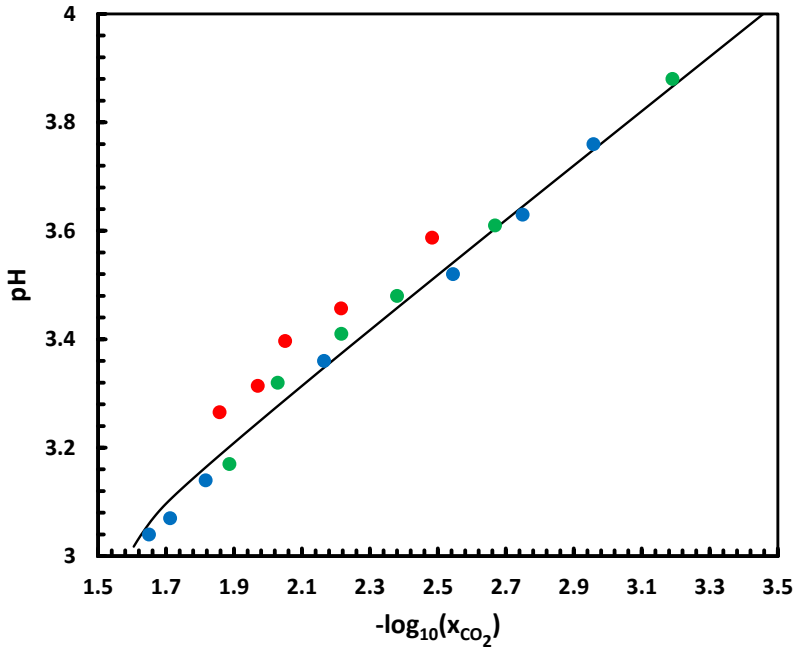

Fig. 14. pH of the CO_2-H_2O system as a function of $-\log_{10}(x_{CO_2})$ at a temperature of 323.15 K. ●, Peng et al. (2013); ●, this work (Spectroscopic technique) and ●, this work (Electrometric technique).

The capability of the model to predict the effect of salts was also investigated. The deviation between the model and experimental data for various CO_2-brine systems are listed in Table 5. The measured pH values in this work for saline systems yield a good agreement with those obtained by the model. The model can reproduce the pH values in the CO_2-H_2O-1m NaCl, CO_2-H_2O-2m NaCl and CO_2-H_2O-3m NaCl systems with AAD of about 0.04-0.10 pH units. Similar to the CO_2-H_2O system, there is a linear dependence among pH and $-\log_{10}(x_{CO_2})$ in the CO_2 saturated brine systems (Fig. 15). Furthermore, low deviations were observed between the model and measured pH points by Shao et al. (2012) in the CO_2-H_2O-3m NaCl system with an AAD of 0.05 pH units., also indicating the adequacy of the model to predict the pH values at a variety of pressure and temperature conditions in highly concentrated NaCl brines. Overall, the model is performing well at various temperature and pressure ranges and various NaCl concentrations.

2

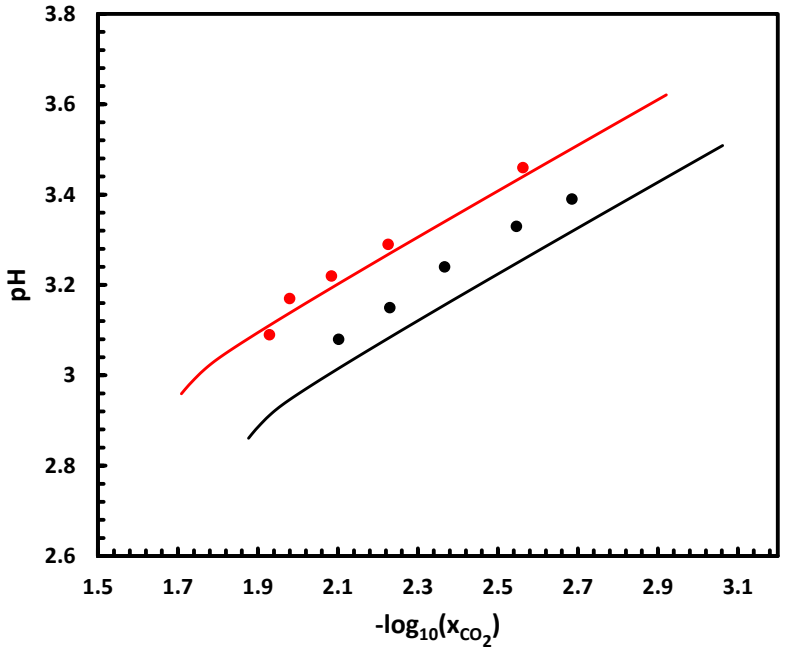

Fig. 15. pH of the CO_2-H_2O-NaCl systems as a function of $-\log_{10}(x_{CO_2})$ at a temperature of 323.15 K (This work, spectroscopic technique). ●, 1m NaCl and ●, 3m NaCl.

6. Conclusions

Two experimental setups based on either electrical or spectroscopic methods were employed to measure the pH at various pressures and temperatures. The pH values were measured for the CO_2-H_2O, CO_2-H_2O-NaCl (NaCl: 1 to 3m) systems at pressures up to 6 MPa and temperatures up to 353.15K. Good agreement was obtained between literature data and measured values. It was shown that the pH of all the studied systems starts to decrease with increasing pressure at each isotherm. According to the spectroscopic, electrometric and modelling results this reduction is sharp while the pressure is less than 3 MPa. This drop in pH value starts to reduce gradually at pressures higher than 3 MPa. Such trends can be explained by the change in solubility of CO_2 in the aqueous phase at different pressure conditions. Moreover, the effect of variation in salinity on pH value was also investigated. It was observed that the pH of CO_2-saturated solutions decreases with an increase in the concentration of NaCl in the solution while the pressure and temperature kept constant.

Furthermore, we described and evaluated a model that uses a robust thermodynamic basis for describing the solubility of gases in the liquid phase and Pitzer's theory for determining the activity coefficients of the ionic species involved. This approach proved to be capable of describing the chemical equilibria of the ionic species in the liquid phase under HPHT

conditions and in systems of interest. The model was tested in concentrated NaCl solutions under CO_2 pressure at realistic industrial operating temperatures. The algorithm presented in this work is prepared to account for the effect of carbon dioxide and the following ionic species: H^+, Na^+, OH^-, Cl^-, HCO_3^- and CO_3^{2-}. All the experimental results for different fluid systems were compared with results that were reproduced by the model to investigate the capability of developed model for different fluid systems. A good agreement between predictions and experimental data is observed. It is noteworthy to mention very small deviations were found at different NaCl concentration, demonstrating the ability of the model to predict the pH in CO_2-brine solutions.

Acknowledgments

This work is part of an ongoing Joint Industrial Project (JIP) at the Institute of Petroleum Engineering, Heriot-Watt University and the CTP laboratory of MINES ParisTech. The JIP was financially funded by Galp Energia, Linde AG, National Grid, Petronas, Statoil and Total which is gratefully acknowledged. The author would also like to thank Jim Allison for his assistance.

Appendix

This section defines the calculations undertaken for uncertainty analysis for both the spectroscopy and electrometric techniques.

1. Uncertainties calculation for the spectroscopy technique:

As mentioned in the manuscript, for the spectroscopy technique, Eq. 8 was used to calculate the pH at various pressure and temperature conditions. Details of calculations used to determine the uncertainties are explained in the following sections for the spectroscopy technique.

a) The e_1, e_2, e_3 and R uncertainties

To calculate the uncertainty of the pH, it is required to first determine the uncertainty of the e_1, e_2, e_3, $R_{\lambda_1}^{\lambda_2}$ and pK_a. Eqs. (23, 25 and 27) were used to calculate the uncertainty of e_1, e_2, e_3 respectively.

$$\frac{U_{e_1}}{e_1} = \sqrt{\left(\frac{\Delta e_A^{\lambda_2}}{e_A^{\lambda_2}}\right)^2 + \left(\frac{\Delta e_A^{\lambda_1}}{e_A^{\lambda_1}}\right)^2} \tag{22}$$

$$U_{e_1} = e_1 \cdot \sqrt{\left(\frac{\Delta e_A^{\lambda_2}}{e_A^{\lambda_2}}\right)^2 + \left(\frac{\Delta e_A^{\lambda_1}}{e_A^{\lambda_1}}\right)^2} \tag{23}$$

$$\frac{U_{e_2}}{e_2} = \sqrt{\left(\frac{\Delta e_B^{\lambda_2}}{e_B^{\lambda_2}}\right)^2 + \left(\frac{\Delta e_A^{\lambda_1}}{e_A^{\lambda_1}}\right)^2} \quad (24)$$

$$U_{e_2} = e_2 \cdot \sqrt{\left(\frac{\Delta e_B^{\lambda_2}}{e_B^{\lambda_2}}\right)^2 + \left(\frac{\Delta e_A^{\lambda_1}}{e_A^{\lambda_1}}\right)^2} \quad (25)$$

$$\frac{U_{e_3}}{e_3} = \sqrt{\left(\frac{\Delta e_B^{\lambda_1}}{e_B^{\lambda_1}}\right)^2 + \left(\frac{\Delta e_A^{\lambda_1}}{e_A^{\lambda_1}}\right)^2} \quad (26)$$

$$U_{e_3} = e_3 \cdot \sqrt{\left(\frac{\Delta e_B^{\lambda_1}}{e_B^{\lambda_1}}\right)^2 + \left(\frac{\Delta e_A^{\lambda_1}}{e_A^{\lambda_1}}\right)^2} \quad (27)$$

Where,

$$\Delta e_A^{\lambda_2} = \Delta e_A^{\lambda_1} = \Delta e_B^{\lambda_2} = \Delta e_B^{\lambda_1} = \sqrt{\left(u_{system}\right)^2 + \left(u_{repeatibility}\right)^2} \quad (28)$$

Therefore, U_{e_1}, U_{e_2} , U_{e_3} were calculated at different temperatures and ionic strengths using equations described in above. The $u_{repeatability}$ for each parameter is equivalent to the standard deviation of five measurements. Moreover, the response of the e_1, e_2 and e_3 to pressure were less than the uncertainty of the measurement.

Eq. (30) used to calculate the uncertainty of the $R_{\lambda_1}^{\lambda_2}$.

$$\frac{U_{R_{\lambda_1}^{\lambda_2}}}{R_{\lambda_1}^{\lambda_2}} = \sqrt{\left(\frac{\Delta A(\lambda_2)}{A(\lambda_2)}\right)^2 + \left(\frac{\Delta A(\lambda_1)}{A(\lambda_1)}\right)^2} \quad (29)$$

$$U_{R_{\lambda_1}^{\lambda_2}} = R_{\lambda_1}^{\lambda_2} \cdot \sqrt{\left(\frac{\Delta A(\lambda_2)}{A(\lambda_2)}\right)^2 + \left(\frac{\Delta A(\lambda_1)}{A(\lambda_1)}\right)^2} \quad (30)$$

Where,

$$\Delta A(\lambda_2) = \Delta A(\lambda_1) = \sqrt{\left(u_{system}\right)^2 + \left(u_{repeatibility}\right)^2} \quad (31)$$

b) pK_a uncertainty

This section describes in detail the calculations undertaken to determine the uncertainty of the pK_a. Eq. (32) used to calculate the pK_a using different standard buffer solutions.

$$pK_a = pH - log\frac{R_{\lambda_1}^{\lambda_2} - e_1}{e_2 - Re_3} \quad (32)$$

Eq. (32) was split into two parts (pH ,$log\frac{R_{\Lambda_1}^{\Lambda_2}-e_1}{e_2-Re_3}$) for ease of calculation.To simplify the second part of the Eq. (32), C_1, C_2, C_3 and C_4 were defined as follows:

$$C_1 = R_{\Lambda_1}^{\Lambda_2} - e_1 \tag{33}$$

$$C_2 = e_2 - Re_3 \tag{34}$$

$$C_3 = \frac{C_2}{C_1} \tag{35}$$

$$C_4 = \log C_3 \tag{36}$$

The uncertainty of C_1, C_2, C_3 and C_4 were then calculated using the following equations:

$$U_{C_1} = \sqrt{\left(\Delta R_{\Lambda_1}^{\Lambda_2}\right)^2 + (\Delta e_1)^2} \tag{37}$$

$$U_{C_2} = \sqrt{(\Delta e_2)^2 + (\Delta Re_3)^2} \tag{38}$$

$$\frac{U_{C_3}}{C_3} = \sqrt{\left(\frac{\Delta C_2}{C_2}\right)^2 + \left(\frac{\Delta C_1}{C_1}\right)^2} \tag{39}$$

$$U_{C_3} = C_3 \cdot \sqrt{\left(\frac{\Delta C_2}{C_2}\right)^2 + \left(\frac{\Delta C_1}{C_1}\right)^2} \tag{40}$$

$$U_{C_4} = \frac{\Delta C_4}{C_4} \tag{41}$$

Eq.(42) used to calculate the uncertainty of the pH measured using the glass electrode (Hanna, HI-2002 Edge®).

$$U_{pH} = \sqrt{\left(u_{system}\right)^2 + (u_{calibration})^2 + \left(u_{repeatibility}\right)^2} \tag{42}$$

$u_{repeatability}$ and u_{system} were calculated to be 0.007 and 0.01 respectively. Moreover, the pH value was changed 0.01 unit, once the change in the e.m.f value was within ± 0.05 mV. Therefore the uncertainty of the calibration is considered to be 0.01. The uncertainty of the pK_a for each temperature and ionic strength was then calculated using Eq. (43).

$$U_{pK_a,C} = \sqrt{\left(U_{pH}\right)^2 + \left(U_{C_4}\right)^2} \tag{43}$$

c) pH uncertainty (spectroscopy technique)

In this section equations used to calculate the uncertainty of the pH measured for the CO_2-H_2O and CO_2-H_2O-NaCl systems using the spectroscopy technique are described in details. Eq. (44) used to calculate the pH of the CO_2- water/brine systems at various pressures.

$$pH = pK_a(t,p,\mu) + log\,\frac{R_{\lambda_1}^{\lambda_2} - e_1}{e_2 - Re_3} \tag{44}$$

As mentioned in the manuscript, pK_a is a function of pressure, temperature and ionic strength. Since the pK_a was determined experimentally at the calibrated temperatures and ionic strengths and the uncertainty of the pK_a was calculated separately at each isotherm and ionic strength, it is also essential to calculate the uncertainty of the pK_a with respect to the pressure. As mentioned in the manuscript Eq. (45) used to correct the pK_a values at various pressures.

$$\frac{RT}{(P-1)}\ln\frac{K_a(t,p,\mu)}{K_a(t,1,\mu)} = -\Delta V + \Delta k\,\frac{P-1}{2} \tag{45}$$

$$K_a(t,p,\mu) = K_a(t,1,\mu)\cdot e^{\frac{-\Delta V(P-1)+\Delta k\,(P-1)^2}{2RT}} \tag{46}$$

Where,

$$pK_a = -\log\left(K_a(t,1,\mu)\cdot e^{\left(\frac{-\Delta V(P-1)+\Delta k\,(P-1)^2}{2RT}\right)}\right) = -\frac{\ln\left(K_a(t,1,\mu)\cdot e^{\left(\frac{-\Delta V(P-1)+\Delta k\,(P-1)^2}{2RT}\right)}\right)}{\ln(10)} \tag{47}$$

$$pK_a = \frac{(-\ln K_a(t,1,\mu)) - \left(\frac{-\Delta V(P-1)+\Delta k\,(P-1)^2}{2RT}\right)}{\ln(10)} \tag{48}$$

Eq. (49) shows the derivative of the pK_a equation with respect to pressure.

$$\frac{dpK_a}{dp} = \frac{\Delta V - 2\cdot\Delta k\,(P-1)}{2RT\cdot\ln(10)} \tag{49}$$

Thus, the uncertainty of the $pK_{a,P}$ was found according to:

$$U_{pK_a,P} = \left|\frac{dpK_a}{dP}\right|\cdot\,\Delta P \tag{50}$$

Where ΔP was found to be approximately 0.05 MPa. The total uncertainty of the pK_a was then calculated by using Eq. (51).

$$U_{pK_a,Total} = \sqrt{\left(U_{pK_a,C}\right)^2 + \left(U_{pK_a,P}\right)^2} \tag{51}$$

Finally, a final combined uncertainty can be calculated using Eq. (52) to estimate the uncertainty of the pH using the spectroscopy technique.

$$U_{\mathrm{pH}} = \sqrt{\left(U_{pK_a,Total}\right)^2 + \left(U_{C_4}\right)^2} \quad (52)$$

2. Uncertainties calculation for the electrometric technique

Eq. (53) used to calculate the uncertainty of the pH for the CO_2-H_2O system.

$$U_{pH} = \sqrt{(u_T)^2 + (u_P)^2 + (u_V)^2} = \sqrt{\left(\left|\frac{dpH}{dT}\right| \cdot \Delta T\right)^2 + \left(\left|\frac{dpH}{dP}\right| \cdot \Delta P\right)^2 + \left(\left|\frac{dpH}{dmV}\right| \cdot \Delta mV\right)^2} \quad (53)$$

References

Aasberg-Petersen, K., Stenby, E., Fredenslund, A., 1991. Prediction of high-pressure gas solubilities in aqueous mixtures of electrolytes. Industrial & engineering chemistry research 30, 2180-2185.

Ahmadi, P., Chapoy, A., Tohidi, B., 2017. Density, speed of sound and derived thermodynamic properties of a synthetic natural gas. Journal of Natural Gas Science and Engineering 40, 249-266.

Babić, S., Horvat, A.J., Pavlović, D.M., Kaštelan-Macan, M., 2007. Determination of pK a values of active pharmaceutical ingredients. TrAC Trends in Analytical Chemistry 26, 1043-1061.

Bates, R.G., Vijh, A.K., 1973. Determination of pH: theory and practice. Journal of The Electrochemical Society 120, 263C-263C.

Briones, J., Mullins, J., Thies, M.C., Kim, B.-U., 1987. Ternary phase equilibria for acetic acid-water mixtures with supercritical carbon dioxide. Fluid Phase Equilibria 36, 235-246.

Carroll, S.A., McNab, W.W., Torres, S.C., 2011. Experimental study of cement-sandstone/shale-brine-CO2 interactions. Geochemical transactions 12, 9.

Chapoy, A., Burgass, R., Tohidi, B., Alsiyabi, I., 2014. Hydrate and phase behavior modeling in CO2-rich pipelines. Journal of Chemical & Engineering Data 60, 447-453.

Chapoy, A., Haghighi, H., Burgass, R., Tohidi, B., 2012. On the phase behaviour of the (carbon dioxide+ water) systems at low temperatures: experimental and modelling. The Journal of Chemical Thermodynamics 47, 6-12.

Clayton, T.D., Byrne, R.H., 1993. Spectrophotometric seawater pH measurements: total hydrogen ion concentration scale calibration of m-cresol purple and at-sea results. Deep Sea Research Part I: Oceanographic Research Papers 40, 2115-2129.

Crabtree, M., Eslinger, D., Fletcher, P., Miller, M., Johnson, A., King, G., 1999. Fighting scale—removal and prevention. Oilfield Review 11, 30-45.

Crolet, J., Bonis, M., 1983. pH measurements in aqueous CO2 solutions under high pressure and temperature. Corrosion 39, 39-46.

Dickson, A., 1984. pH scales and proton-transfer reactions in saline media such as sea water. Geochimica Et Cosmochimica Acta 48, 2299-2308.

Foti, C., Rigano, C., Sammartano, S., 1999. Analysis of thermodynamic data for complex formation: Protonation of THAM and fluoride ion at different temperatures and ionic strengths. Annali di chimica 89, 87-98.
Gaus, I., 2010. Role and impact of CO 2–rock interactions during CO 2 storage in sedimentary rocks. International journal of greenhouse gas control 4, 73-89.
Gray, L.G., Anderson, B.G., Danysh, M.J., Tremaine, P., 1989. Mechanism of carbon steel corrosion in brines containing dissolved carbon dioxide at pH 4. Corrosion/89, paper.
Gray, S.E.C., DeGrandpre, M.D., Moore, T.S., Martz, T.R., Friederich, G.E., Johnson, K.S., 2011. Applications of in situ pH measurements for inorganic carbon calculations. Marine Chemistry 125, 82-90.
Haghighi, H., Chapoy, A., Tohidi, B., 2008. Freezing point depression of electrolyte solutions: experimental measurements and modeling using the cubic-plus-association equation of state. Industrial & Engineering Chemistry Research 47, 3983-3989.
Haghighi, H., Chapoy, A., Tohidi, B., 2009. Methane and water phase equilibria in the presence of single and mixed electrolyte solutions using the cubic-plus-association equation of state. Oil & Gas Science and Technology-Revue de l'IFP 64, 141-154.
Hou, S.-X., Maitland, G.C., Trusler, J.M., 2013a. Measurement and modeling of the phase behavior of the (carbon dioxide+ water) mixture at temperatures from 298.15 K to 448.15 K. The Journal of Supercritical Fluids 73, 87-96.
Hou, S.-X., Maitland, G.C., Trusler, J.M., 2013b. Phase equilibria of (CO 2+ H 2 O+ NaCl) and (CO 2+ H 2 O+ KCl): measurements and modeling. The Journal of Supercritical Fluids 78, 78-88.
Huang, S.H., Radosz, M., 1990. Equation of state for small, large, polydisperse, and associating molecules. Industrial & Engineering Chemistry Research 29, 2284-2294.
Kakiuchi, T., 2011. Salt bridge in electroanalytical chemistry: Past, present, and future. Journal of Solid State Electrochemistry 15, 1661-1671.
Kontogeorgis, G.M., Michelsen, M.L., Folas, G.K., Derawi, S., von Solms, N., Stenby, E.H., 2006a. Ten years with the CPA (Cubic-Plus-Association) equation of state. Part 1. Pure compounds and self-associating systems. Industrial & engineering chemistry research 45, 4855-4868.
Kontogeorgis, G.M., Michelsen, M.L., Folas, G.K., Derawi, S., von Solms, N., Stenby, E.H., 2006b. Ten years with the CPA (Cubic-Plus-Association) equation of state. Part 2. Cross-associating and multicomponent systems. Industrial & engineering chemistry research 45, 4869-4878.
Kontogeorgis, G.M., Voutsas, E.C., Yakoumis, I.V., Tassios, D.P., 1996. An equation of state for associating fluids. Industrial & engineering chemistry research 35, 4310-4318.
Marion, G., Millero, F., Camões, M., Spitzer, P., Feistel, R., Chen, C.-T., 2011. pH of seawater. Marine Chemistry 126, 89-96.
Mathews, S.G., Raghuraman, B., Rosiere, D.W., Wei, W., Colacelli, S., Rehman, H.A., 2009. Laboratory Measurement of pH of Live Waters at High Temperatures and Pressures, SPE International Symposium on Oilfield Chemistry. Society of Petroleum Engineers.
Meyssami, B., Balaban, M.O., Teixeira, A.A., 1992. Prediction of pH in model systems pressurized with carbon dioxide. Biotechnology progress 8, 149-154.
Millero, F.J., DiTrolio, B., Suarez, A.F., Lando, G., 2009. Spectroscopic measurements of the pH in NaCl brines. Geochimica et Cosmochimica Acta 73, 3109-3114.
Parkhurst, D.L., Appelo, C., 1999. User's guide to PHREEQC (Version 2): A computer program for speciation, batch-reaction, one-dimensional transport, and inverse geochemical calculations.
Parton, T., Spilimbergo, S., Elvassore, N., Bertucco, A., 2002. UV-vis spectroscopy for the determination of diffusion coefficient and pH in aqueous solutions/SC–CO2 systems, High

Pressure in Venice 4th International Symposium on High Pressure Process Technology and Chemical Engineering.
Pedersen, K.S., Christensen, P.L., Shaikh, J.A., 2014. Phase behavior of petroleum reservoir fluids. CRC Press.
Peng, C., 2015. Chemical Interactions Between CO2 Acidified Aqueous Fluids and Carbonate Minerals.
Peng, C., Crawshaw, J.P., Maitland, G.C., Trusler, J.M., Vega-Maza, D., 2013. The pH of CO 2-saturated water at temperatures between 308K and 423K at pressures up to 15MPa. The Journal of Supercritical Fluids 82, 129-137.
Pitzer, K.S., 1973. Thermodynamics of electrolytes. I. Theoretical basis and general equations. The Journal of Physical Chemistry 77, 268-277.
Pitzer, K.S., Peiper, J.C., Busey, R., 1984. Thermodynamic properties of aqueous sodium chloride solutions. Journal of Physical and Chemical Reference Data 13, 1-102.
Poling, B.E., Prausnitz, J.M., John Paul, O.C., Reid, R.C., 2001. The properties of gases and liquids. McGraw-Hill New York.
Raghuraman, B., Gustavson, G., Van Hal, R., Dressaire, E., Zhdaneev, O., 2006. Extended-range spectroscopic pH measurement using optimized mixtures of dyes. Applied spectroscopy 60, 1461-1468.
Robert-Baldo, G.L., Morris, M.J., Byrne, R.H., 1985. Spectrophotometric determination of seawater pH using phenol red. Analytical Chemistry 57, 2564-2567.
Rosenqvist, J., Kilpatrick, A.D., Yardley, B.W., 2012. Solubility of carbon dioxide in aqueous fluids and mineral suspensions at 294K and subcritical pressures. Applied geochemistry 27, 1610-1614.
Schaef, H.T., McGrail, B.P., Martin, P.F., 2003. Direct measurements of pH and dissolved CO2 concentrations in H2O-CO2-NaCl mixtures to supercritical conditions, Carbon Sequestration Second Annual Conference, Alexandria, Virginia.
Shao, H., Thompson, C.J., Cantrell, K.J., 2013. Evaluation of experimentally measured and model-calculated pH for rock–brine–CO 2 systems under geologic CO 2 sequestration conditions. Chemical Geology 359, 116-124.
Shao, H., Thompson, C.J., Qafoku, O., Cantrell, K.J., 2012. In situ spectrophotometric determination of pH under geologic CO2 sequestration conditions: method development and application. Environmental science & technology 47, 63-70.
Shibata, M., Sakaida, H., Kakiuchi, T., 2010. Determination of the activity of hydrogen ions in dilute sulfuric acids by use of an ionic liquid salt bridge sandwiched by two hydrogen electrodes. Analytical chemistry 83, 164-168.
Shinwari, M.W., Zhitomirsky, D., Deen, I.A., Selvaganapathy, P.R., Deen, M.J., Landheer, D., 2010. Microfabricated reference electrodes and their biosensing applications. Sensors 10, 1679-1715.
Toews, K.L., Shroll, R.M., Wai, C.M., Smart, N.G., 1995. pH-defining equilibrium between water and supercritical CO2. Influence on SFE of organics and metal chelates. Analytical Chemistry 67, 4040-4043.
Truche, L., Bazarkina, E.F., Berger, G., Caumon, M.-C., Bessaque, G., Dubessy, J., 2016. Direct measurement of CO 2 solubility and pH in NaCl hydrothermal solutions by combining in-situ potentiometry and Raman spectroscopy up to 280° C and 150bar. Geochimica et Cosmochimica Acta 177, 238-253.
Usha, A., Atkinson, G., 1992. The effect of pressure on the dissociation constant of hydrofluoric acid and the association constant of the NaF ion pair at 25° C. Journal of solution chemistry 21, 477-488.
Waters, J.F., Millero, F.J., 2013. The free proton concentration scale for seawater pH. Marine Chemistry 149, 8-22.

Wiebe, R., 1941. The Binary System Carbon Dioxide-Water under Pressure. Chemical reviews 29, 475-481.
Yamada, A., Mohri, S., Nakamura, M., Naruse, K., 2015. A Simple Method for Decreasing the Liquid Junction Potential in a Flow-through-Type Differential pH Sensor Probe Consisting of pH-FETs by Exerting Spatiotemporal Control of the Liquid Junction. Sensors 15, 7898-7912.
Zaalishvili, S., 1940. The solubility of carbon dioxide mixed with hydrogen and nitrogen in water under pressure. Zh. F iz. Khim 14, 413-417.
Zawisza, A., Malesinska, B., 1981. Solubility of carbon dioxide in liquid water and of water in gaseous carbon dioxide in the range 0.2-5 MPa and at temperatures up to 473 K. Journal of Chemical and Engineering Data 26, 388-391.
Zhang, H., Byrne, R.H., 1996. Spectrophotometric pH measurements of surface seawater at in-situ conditions: absorbance and protonation behavior of thymol blue. Marine Chemistry 52, 17-25.